Two Higgs Doublets plus One Dark Matter Singlet

Alexey Tochin

Thesis for the degree of
Master of Science
in Elementary Particle Physics

Department of Physics and Technology
University of Bergen
Norway

August 2010

Acknowledgments

I want to thank much my adviser Per Osland for the support and direction that he has given me. I greatly appreciate the help of Mahdi Purmohammadi in technical support. I also would like to thank University of Bergen, the Faculty of Mathematics and Natural Sciences and Department of Physics and Technology for the acceptance to the Master's degree program. In fact this work was supported by the Norwegian State Educational Loan Fund.

Contents

Introduction

In this thesis an extension of the 2HDM (see chapter 2) is explored. The extension admits an extra inert singlet which is a dark matter candidate. Before the exploration a large part of the thesis (chapter 1) is an overview of dark matter theory that includes the evidence of dark matter existence, list of the most popular candidates, information of experimental detection and others. The phenomenology of the relic abundance is discussed in detail.

Scanning over parameters of the considered model the abundance of the dark matter is constrained in agreement with WMAP data. Imposing all relevant collider and theoretical constraints the allowed parameter space for which dark matter is appropriate will be determined.

It is done using two methods. The first one is to draw histograms of allowed regions with some parameters fixed and others are arbitrary (chapter 3). The second method is to draw scatter plots where all parameters are random (chapter 4). The important case of the theory with quadratic divergency cancellation will be discussed in chapter 4 together with the usual one.

Some attempts to use different numerical methods (appendices A and B) of searching for such allowed regions in the parametric space are presented. But it is rather a training of them than an active application or at least an attempt to find any new method of the calculation optimization.

Chapter 1

Dark matter

This chapter will be about general Dark matter (DM) information. It may be found in a great amount of literature, in particular [1, 2, 3, 4] and others. This is just a short summary of this material. In the first subsection the evidence for DM will be discussed. The second one is about general important properties and necessary condition of any DM theory. The most popular of such theories will be listed in the third subsection. And in the fourth part of this section some experimental results will be presented. The phenomenology of DM relic abundance plays an important role in the present investigation and will be discussed in detail in the last section.

1.1 Observational evidence

A series of astronomical observations indicate that not all matter in the universe is visible. It is intended to be read that not all matter which is visible through its gravitational effects can be detected through electromagnetic emission as known kinds of baryonic matter. This hypothetical form of matter was called "dark matter". This term was coined by Fritz Zwicky in 1934 who is the "Father of Dark Matter". But besides of "darkness" it is also utterly transparent at least for the largest part of dark matter models.

It is convenient to measure an amount of any kind of matter in the Universe as

$$\Omega_X = \frac{\rho_X}{\rho_c} \ , \tag{1.1}$$

where

$$\rho_c = \frac{3H^2}{8\pi G} \ . \tag{1.2}$$

is the critical density which is the value at which in accordance with the Friedman model the Universe is at balance, and expansion is stopped.

So the mass of visible (luminous) matter (stars, gas etc.) is estimated as

$$\Omega_{\rm lum} < 0.003h^{-1} = 0.003...0.007 \ , \tag{1.3}$$

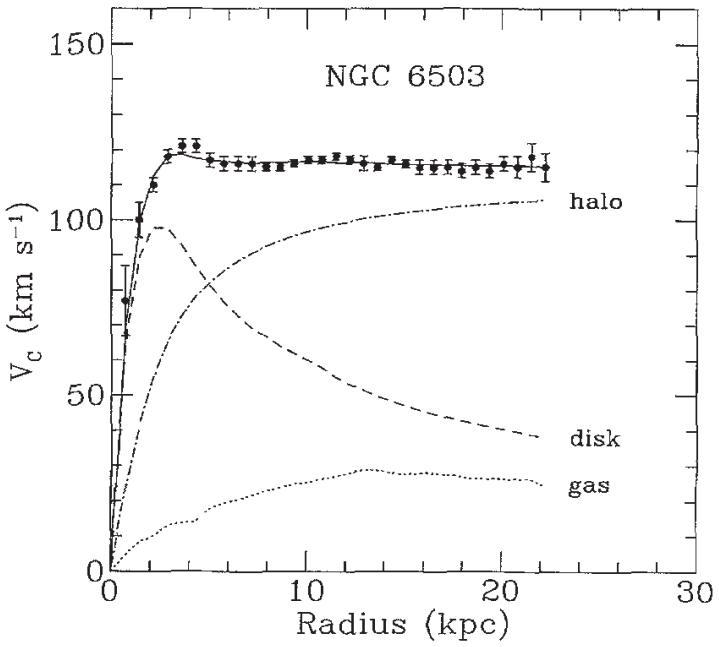

Figure 1.1: Rotational curve for the spiral galaxy NGC 6503. The points are the measured circular rotation velocities as a function of distance from the center of the galaxy. The dashed and dotted curves are the contributions to the rotational velocity due to the observed disk and gas, respectively, and the dot-dashed curve is the contribution from the dark halo. (From [2] with a reference to [5].)

where $h = 0.4-1$ parameterizes the uncertainty in the Hubble constant, $H_0 = 100h$ km^{2}s^{-1}Mpc^{-1}.

There is a great amount of experimental evidence for dark matter [1, 2, 3, 4]. This evidence can be classified by the physical principles of the investigation, space scale or historical order. This is just a review of the first way.

- **Galactic rotation curves [5]**

  From the observation of spiral galaxies it appears that the velocity of stars and gas rotation speed decrease too slowly with the distance from the centre. It may be explained as a result of the presence of extra invisible matter in the galactic halo.

  For an example, see fig. 1.1. This galaxy is typical. So from [6]

  $$\Omega_{\rm halo} > 0.017 \ . \tag{1.4}$$

  The same situation is with external galaxy rotation. Using as example of satellite galaxies around spirals similar to the Milky Way, Zaritsky [7] estimated the total mass of a "typical" spiral. It implies

  $$\Omega_{\rm spiral} \gtrsim 0.087 h^{-1} \tag{1.5}$$

in the space which is outside of the spirals. It is interesting that there is no strong evidence that rotation speed decreases with the investigated satellites radius. So it is only an upper limit.

- **Velocity dispersions of galaxies**

  This is an evaluation of the measurements of velocity curves in spiral galaxies. More detail and exact method is for example connected with velocity dispersions of elliptical galaxies [10].

  The fraction of the total amount of gravitational matter is found to be about 95% which is now the accepted value. Furthermore it was found that the distribution of dark matter is not so homogeneous. In particular in 2005 a galaxy made almost entirely of dark matter was found (VIRGOHI21) [11]. On the other hand there are small galaxies which velocity profile indicate an absence of dark matter, for instance NGC 3379 [12].

- **Galaxy clusters and gravitational lensing**

  The light from a distant source is bent around a cluster of galaxies which is a sufficiently massive object to generate a detectable specific effect that is known as gravitational lensing. In accordance with gravitational theory the background picture must be deformed. From such consideration the visible mass is at most only 13% of the estimated one [13].

- **Galaxy clusters collision observation**

  In the process of galaxy cluster collision the visible matter deforms its space distribution. But dark matter halo does not because its interaction with both kinds of matter is weak. A numerical calculation of the galaxy collision process gives us an obvious picture of collided visible matter distribution. This picture is in wonderful accordance with the one estimated from gravitational lensing [14, 15, 16].

- **Anisotropy of the Cosmic Microwave Background (CMB)**

  The anisotropy of the CMB is determined by two factors: acoustic oscillations and diffusion damping. The pressure of the photons tends to erase anisotropies (diffusion) but the gravitation of baryon matter which is moving at speeds much slower than light collapse them to form dense haloes. This effect leads to a characteristic peak structure of the CMB power spectrum (see fig. 1.2) [20]. The first peak is connected with the curvature of the Universe. The second one is connected with baryon density. The third peak can be used to extract information about the dark matter density.

There are also some attempts to modify the theory of gravitation, like [17, 19] to explain the gravitationally based discrepancies which would be more elegant. But they are not successful yet. Furthermore a large family of different arguments leads to the similar order of the amount of dark matter and the argument about galaxy clusters collision observation is too convincing for non dark matter explanation [21, 22].

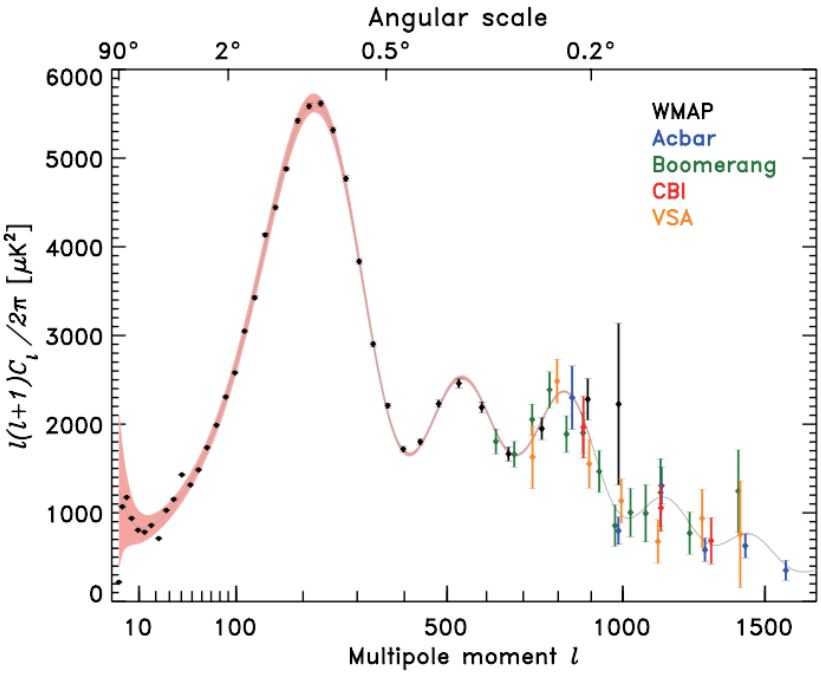

Figure 1.2: The power spectrum of the cosmic microwave background radiation temperature anisotropy in terms of the angular scale (or multipole moment). The data shown come from the WMAP (2006), Acbar (2004) Boomerang (2005), CBI (2004), and VSA (2004) instruments. Also shown is a theoretical model (solid line). From [20].

1.2 Ten points for a new DM particle

Before giving a list of DM candidates let us discuss the main requirements for them.

In [3] a ten-point test that a new particle has to pass, in order to be considered a viable DM candidate is presented. This section is structured in accordance with these ten questions. The answers for the two Higgs doublet plus 1 inert singlet model (see chapter 2) which is the subject of the present thesis will be given separately.

1. **Does it match the appropriate relic density?** For some cases such as exotic baryonic candidates this question is solved individually and often connected with Big Bang Nucleosynthesis (BBN). For other types of DM such weakly interacting particles (WIMP) and in particular the present case (2HDM+1S) this theory will be presented in sec. 1.5. This test plays the main role in the present investigation of the model.

2. **Is it cold?** DM is called "cold"(CDM) if the particles moved at nonrelativistic speed at freeze-out epoch (see sec. 1.5). And it is called "hot" if the speed was relativistic. There is also term the "warm" DM for the intermediate case with mass of order 1

keV. Hot DM in distinction from cold one cannot cluster on galaxy scales until it has cooled to nonrelativistic speeds. So it leads to different primordial fluctuation spectrum (see the previous section). The typical example of hot DM is the light neutrino. Gravitinos in gauge-mediated supersymmetry breaking models might be warm DM. The cold one is the most popular choice and is the present one.

3. **Is it neutral?** In spite of the often stated condition for DM to not take part in electromagnetic and strong interactions there are some investigations that consider such scenarios. The typical example is CHAMP (see 1.3). The singlet field in the 2HDM is neutral.

4. **Is it consistent with BBN?** The SM predicts in particular a baryon to photon ratio η with fairly high accuracy (95%) [23]. An extension of the SM may affect that. For example, the presence of a new light particle may change the effective relativistic degrees of freedom g_* (see sec. 1.5) for the epoch of nucleosynthesis $T \sim 1$ MeV. In the case of the 2HDM the new particles are sufficiently heavy (of order $10-100$ GeV) to not change this parameter so this test should be OK for the present model.

5. **Does it leave stellar evolution unchanged?** If a weakly interacting particle is light, it may be produced in the hot plasma of stars. Escaping without further interactions it represents an energy loss channel that may modify the stellar evolution. It is very sensitive to fractionally charged particles (see 1.3). Furthermore DM annihilations may provide an important source of energy that may be comparable to the one from nuclear reactions in the case of small stars [24]. Analysis for the case of the 2HDM+1S is not considered here.

6. **Is it compatible with constraints on self-interactions?** For the collisionless CDM there is a conflict between the cuspy DM halos predicted by N-body simulations and the constant core profiles (see "Galactic rotation curves" in the previous section). Possible solutions are "warm" DM (see point 2) and self-interacting DM (SIDM). If the particle has large elastic scattering cross section the central cusp reduces to an almost constant core [31]. In the 2HDM+1S the self-coupling parameter λ_ϕ (see sec. 2.2) is actually arbitrary (but it is bounded by unitarity (see sec. 2.4.1)). So this problem can in principle be fixed but the analysis is quite involved and will not be done here.

7. **Is it consistent with direct DM searches?** This question will be discussed in section 1.4.1. For the case of the 2HDM+1S it will not be done here.

8. **Is it compatible with gamma-ray constraints?** This question will be discussed in section 1.4.2. For the case of 2HDM+1S it will not be done here.

9. **Is it compatible with other astrophysical bounds?** This question will be discussed in section 1.4.2. For the case of the 2HDM+1S it will not be done here.

10. **Can it be probed experimentally?** Some DM candidates such as gravitino and axino interact too weakly with SM matter and can hardly be detected. In order to have a good physical model one can add a condition of "discoverability". This point is individual for each model. A model with DM candidates that may be probed in the near future experiments are usually the most popular. For the case of the 2HDM+1S this analysis will not be done here.

There are of course also many restrictions for any model itself due to theoretical and experimental (in accelerators) requirements that are not connected with astrophysics. They are obviously individual and for the case of the 2HDM+1S will be discussed in section 2.4.2.

1.3 Dark matter candidates

"It is fairly easy to invent a DM relic, it is much (!) harder to invent a (lasting) model of 'new physics' "[1]

An overview of different DM candidates is given in for example [4, 2]. This is just a brief review of all (that the author has found) DM candidates and corresponding models.

1. WIMPs (weakly interacting massive particles)

   This term is used for a group of DM candidates (the most popular ones) which consist of theories with a DM particle that interacts weakly. It is a natural solution when the DM can not by its very definition take part in electromagnetic interaction. Furthermore it should preferably not interact strongly. These particles as expected can be generated immediately after the Big Bang.

   It is the most popular candidates of DM. WIMPs must be stable particles (in some case just long lived such that the life time is comparable with the age of the Universe).

   (a) **Neutrino**

      i. **SM neutrino**
      This stable particle is the most abundant in the universe after relic photons. Since the SM neutrino indeed is a massive particle it contributes to the DM density. The maximum contribution can be calculated from the Big Bang cosmology [25]

      $$\Omega_\nu h^2 = \frac{\sum_i m_{\nu_i}}{94 \text{ eV}} \ . \tag{1.6}$$

      From the experimental restrictions on neutrino masses follows

      $$\Omega_\nu h^2 < 0.07 \ . \tag{1.7}$$

      So it is only a small part of the necessary value.

[1] Leszek Roszkowski, from presentation "Dark Matter" (Spaatind 2010, Nordic Conference in Particle Physics).

ii. **Sterile neutrinos**
These are extra fermion particles that do not take part in electro-weak interactions but can mix with SM neutrinos. Such SM extension can solve contradiction in experiments of neutrino oscillations. As DM candidates these particles were suggested in [26].
Their lifetime may be larger than the age of the Universe. Experimental results give the restriction for the mass [37]

$$m_{\text{ster}} \geq 14 \text{ keV} .$$

iii. **Heavy and very heavy neutrinos**
There are some models with heavy and very heavy neutrinos. For example [27] with natural fourth generation heavy neutrino. Its mass must be

$$45 \text{ GeV} \leq m_{\nu_H} \leq 1 \text{ TeV}$$

The lower limit is from the LEP experiment [4]. The upper one is from perturbative unitarity.

(b) **Supersymmetric particles.**
Supersymmetric theory (in particular MSSM) is the most popular extension of the SM and gives the most popular DM candidates. Due to R-parity conservation the lightest supersymmetric particle (LSP) is stable and is a good DM candidate. The next to lightest supersymmetric particle (NLSP) could be long-lived which leads to interesting collider signatures [3].

i. **Neutralino.** This is a linear combination of superpartners of gauge bosons and Higgs particles with spin $\frac{1}{2}$. It is the most popular DM candidate.

ii. **Gravitino.** This is a superpartner of the graviton in theories with supergravity and has spin $\frac{3}{2}$. Due to only gravity interaction of the gravitino it is not an interesting candidate of direct and indirect DM search experiments [60].

iii. **Axino.** This particle appears in supersymmetric models implementing the Peccei-Quinn mechanism for solving the strong CP problem. As it appears from the name, Axino is a superpartner of the Axion. Its mass ranges from the eV to the GeV scale. Direct detection and collider production are strongly suppressed [59].

(c) **Inert Higgs models.** Using different SM extensions in the Higgs sector it is possible to have a scalar DM candidate. This is the topic of the present thesis.

(d) **WIMPZILLAS.** This is a very heavy ($m_\chi \leq 10^{13}$ GeV) WIMP which was not in thermodynamical equilibrium in the early universe [32].

(e) **Axion.** This emerges from a possible solution to the strong CP problem [41, 42]. Its mass must be $m \sim 10^{-5}$eV. If axions exist in our halo, they may be detected via resonant conversion to photons in a magnetic field. There is also a pseudo-Nambu-Goldstone boson, similar to the axion, that can be a DM candidate.

2. **Exotic baryon candidates**

   (a) **MACHOs** (Massive compact halo objects) [38]
   These include:

      i. **Brown dwarfs.**
      They are balls of H and He with masses less than $0.08M_{\odot}$, and they never begin nuclear fusion of hydrogen.

      ii. **Jupiters.**
      It is the same as brown dwarfs but with masses of order $0.001M_{\odot}$.

      iii. **Stellar black hole.**
      Masses are near $100M_{\odot}$. They may be remnants of an early generation of stars.

      iv. **White dwarfs.**

      v. **Neutron stars.**

   Of course there are some restriction like the Big Bang nucleosynthesis constraint. Furthermore there are several theoretical [39] and experimental [40] arguments against the dark matter consisting entirely of MACHOs.

   (b) **Strangelets and nuclearites.** Strangelets are particles (of course hypothetical) that consist of a bound state of roughly equal numbers of u, d and s quarks [56]. The size may be about a light nucleus or macroscopic of order meters. In the second case they are called quark stars or "strange stars". A state of positively charged strangelet surrounded by electrons is called nuclearite. In an aerostatic experiment [57] there is a hint of the existence of fast massive charged particles in cosmic rays.

   (c) **Technibaryons.** The idea of technicolor and technimatter may be used as well as the idea of strange matter for the DM problem. Technibaryon must have mass around 1 TeV [58].

   (d) **CHAMP.** This is a charged massive particle. In [28] a hypothetical particle with positive or negative electric charge was suggested as a DM candidate. Positive ones can capture an electron to form a bound state which is chemically equivalent to hydrogen. This leads to the existence of "heavy water" XHO that can be found in the Earth oceans. The negative CHAMP can instead bind to an α^{++} particle and an electron, which leads to heavy-hydrogen-like atom again. There are a lot of experiments that excluded the existence of CHAMP with mass between 10^2 GeV and 10^{16} GeV [4].

   (e) **Fractionally electric charge particles.** Theoretical frameworks have been proposed where particles with fractional electric charge exist (see for example [29]). From the experiment the region with $m < 1$ keV and $q > 10^{-5}e$ was excluded.

(f) **SIMP.** Strongly interacting massive particle. In principle, the DM particle could have an $SU(3)_c$ charge and be "colored" (see for example [30]). In the framework of such models colored particles can be stable. Of course there are many essential experimental restrictions [3]. However very heavy such particles with mass of order $10^{20} - 10^{33}$ GeV can exist without contradiction with experiment.

(g) **SIMPZILLA.** This is just a strongly interaction analogue of WIMPZILLA [33].

(h) **SUSY Q-balls.** In the frameworks of supersymmetric theories there exist nontopological solitons. It is a coherent state of squarks, sleptons and Higgs field that can have large baryon number ($Q_B \leq 10^{24}$) and be rather heavy ($m \approx 1$ TeV). Such particles are absolutely stable and can be generated in the early universe [53].

(i) **Crypto-baryon candidates.** The idea of crypto-baryon matter (for example [54]) is that there exist at least one other phase of the vacuum degenerate with the usual one. The DM is a phase of the matter which is a compressed set of atoms with a size of order 20 cm. The mass of such an object may be of order of 10^{11} kg.

(j) **Magnetic monopoles.** The idea of magnetic monopoles was first discussed by Dirac. Now such hypothetical particles in the framework of different models may have mass of order 1 GeV, 10^{17} GeV in GUT [55] and $10^7 - 10^{13}$ GeV in some modifications [1]. Such particles were not found experimentally. The best experimental limits for the monopole DM flux is from the MACRO, $\Phi < 1,4 \cdot 10^{-16}\text{cm}^{-2}\text{c}^{-1}\text{cp}^{-1}$ [34].

(k) **Mirror matter.** The idea of mirror matter [35] is that there is a "second SM" with particles that almost do not interact with ordinary SM particles but has the opposite CP-symmetry breaking. The interaction between the two kinds of matter is only gravitational or in some modification is in phonon, neutrino or Higgs particles mixing [36]. The important difference of this kind of DM is a rich self-interaction.

This list may prove for someone that the fantasy of people is much more rich than any experimental ability to limit it.

1.4 Detection of dark matter particles

1.4.1 Direct detection

WIMP dark matter particles (if they exist) can in principle be detected directly through detection of elastic scattering with nuclei.

WIMP-nuclei interactions can be split into spin independent (SI) (scalar) and spin dependent (SD) interactions. For example a scalar DM particle (which is the case of the

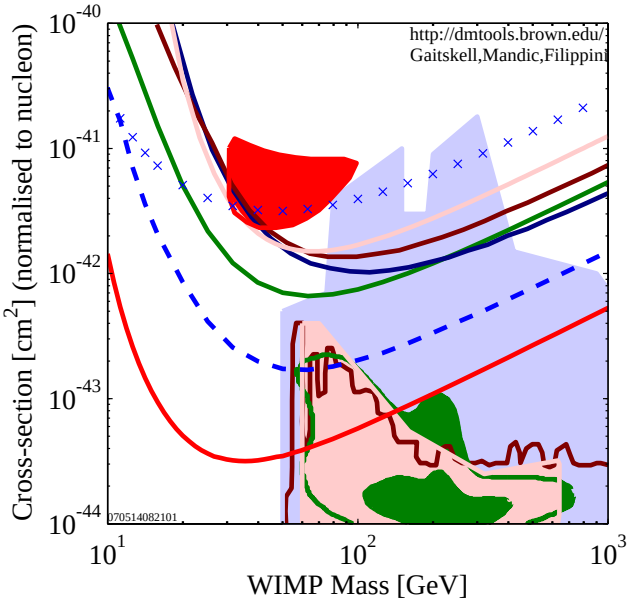

Figure 1.3: Upper limits on the spin independent WIMP-nucleon cross section, versus WIMP mass. The blue dashed (points) line is the Ge (Si) CDMS bound. The dark red, pink, green and dark blue curves are the experimental limits respectively from EDELWEISS and WARP. The lowest red solid line shows the first results from XENON 10. The red shaded region is the parameter space favored by the DAMA experiment. Supersymmetric models allow the filled regions colored: pink, green, dark red and blue. This figure has been obtained with the use of the interface at http://dendera.berkeley.edu/plotter/entryform.html. From [3].

present thesis) can only have a spin-independent interaction. Detectors made of heavy nuclei (for example Germanium, Xenon) are the best for probing the scalar interaction but they also have a sensitivity to the spin-dependent one. The sensitivity of both types of detectors for spin dependent interaction is similar.

Many experiments involving a variety of nuclei have been set up or are being planned. An overview of SI results is presented in fig. 1.3, the same for SD results in fig. 1.4.

1.4.2 Indirect detection

If DM particle exists and can annihilate the products in principle can be detectable. The annihilation must be most active in areas of high concentration which should be galactic centers and star cores and even the Earth interior where WIMPs can be accumulated. Four types of annihilation product are usually distinguished.

- **Gamma-ray**

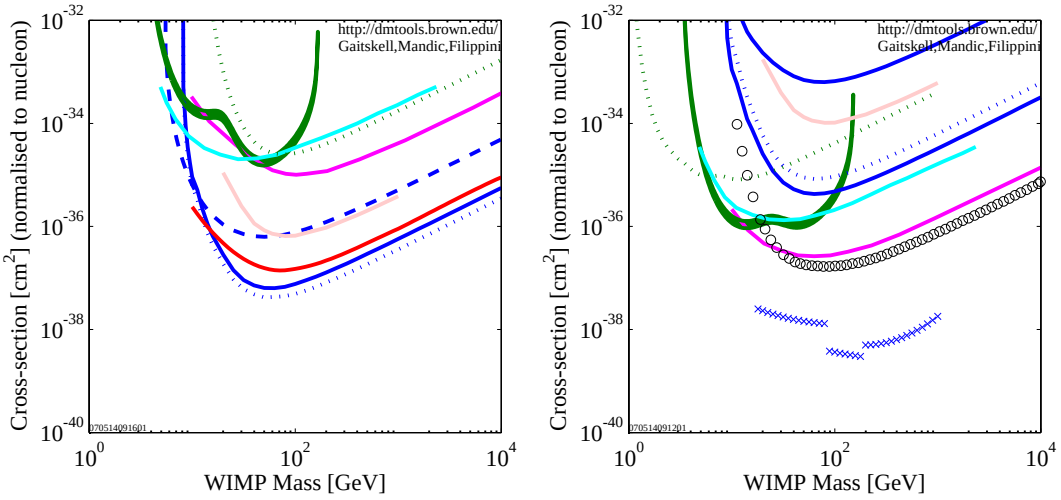

Figure 1.4: Upper limits on spin-dependent WIMP cross section as a function of the WIMP mass, in the case of a pure neutron (left) and proton (right) coupling. The solid (dashed) blue line is the Ge (Si) CDMS bound. The dotted blue line is the CDMS limit with an alternative form factor. The light red, cyan, magenta and red curves are the experimental limits respectively from EDELWEISS, PICASSO, NAIAD 2005 and ZEPLIN I. The dark green shaded region shows the parameter space favored by DAMA experiments. Finally the green points represent the CRESST results, the black crosses stand for Super-Kamiokande and the black circles for KIMS 2007. The figures have been obtained with the use of the interface at http://dendera.berkeley.edu/plotter/entryform.html. From [3].

Photons of energies from 1 GeV to 1 TeV, can not be detected near the Earth surface because almost all of them are absorbed by the atmosphere. So direct detectors such as PAMELA and GLAST are on satellites. Another way is to detect Cherenkov light from electromagnetic cascade from the interaction of the photon in the atmosphere. This is the idea of CANGAROO, HESS, MAGIC and VERITAS. Observations of gamma-ray energy band of 50 keV - 1 MeV have been performed by Osse experiments [61], INTEGRAL [51] and others. The results for the spectrum of the inner Galactic plane are presented in fig. 1.5. This figure shows that there is no conclusive evidence for DM annihilations. But it is remarkable that the Galactic center is a source of gamma rays in the 1 TeV region, which are unexplainable by known SM processes. This in particular can be interpreted as DM annihilation.

There are also some observations of extragalactic gamma-ray background (EGB) by EGRET and others and a bump at a few GeV has been found. It can also be interpreted as DM annihilation. However this can not be considered as evidence of DM since an arbitrariness in DM parameters allow enough freedom to explain almost any excess [50].

By INTEGRAL a 511 keV emission line towards the galactic center was also discov-

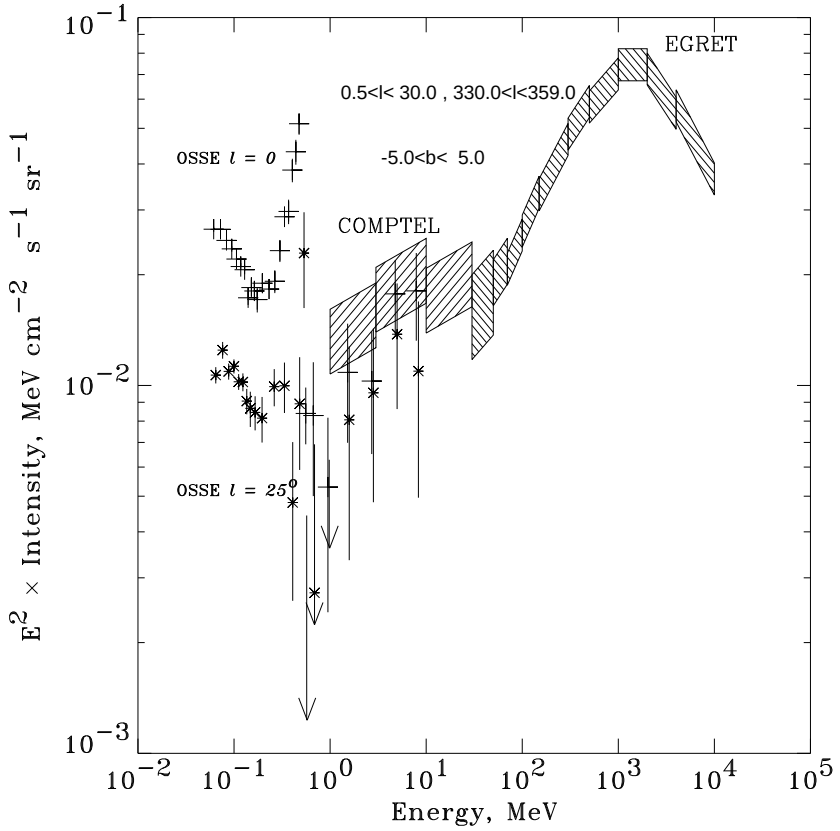

Figure 1.5: Photon spectrum from the inner Galactic plane measured by different experiments for energies ranging from sub MeV up to tens of GeV. From Ref. [3] and [49].

ered. It coincides with positron annihilation. But the size and morphology of the line can hardly be explained by conventional astrophysical scenarios [51]. One of the solutions is WIMP DM models for example [52].

- **Neutrinos**

  Neutrinos, as very weakly interacting particles are almost not absorbed by the Earth and Sun in contradiction to other SM particles. So the excess of neutrino flux from the Galactic center, Sun and Earth interior can be a good experimental confirmation of the DM theory.

  1. **Super Kamiokande.** On the basis of such detection (actually absence of any results of such high energy neutrino detection) strong restrictions on WIMPs was obtained [43].

2. **MACRO, AMANDA and others.** In [44, 46] the restrictions from muons that are generated from the neutrino flux were published.
3. **IceCube, ANTARES, NESTOR, NEMO, KM3NeT and others.** They may give more results for DM annihilation rate or at least prove the possibility to do it.

- **Antimatter**

  Antimatter SM particles can also be produced in DM annihilation and be measurable as an exotic contribution in the spectra in cosmic-ray fluxes. But due to the interaction with interstellar magnetic fields it cannot give information about their source.

  The HEAT experiment has observed an excess of positrons, with respect to standard propagation models, at energies beyond 7 GeV [47]. This result has been confirmed by further measurements (HEAT and AMS-01 data). It may by explained in particular in the framework of supersymmetry and Kaluza-Klein DM.

  An analysis of antiproton excess can also be done. In particular the data collected by BESS, CAPRICE and BESS-Polar. This does not show evidence of primary antiprotons and is not even a constraint on DM candidate because of large uncertainties [48].

  Much more data will be available from BESS-Polar, PAMELA and AMS-02.

1.5 DM relic abundance calculation

1.5.1 Derivation of the Boltzmann equation

An idea of the genesis of WIMP Dark matter is that it was kept in thermal equilibrium with SM (or any of its extension) visible matter because of the process

$$\chi + \bar{\chi} \leftrightarrow X + \bar{X}, \tag{1.8}$$

where χ ($\bar{\chi}$) is a DM particle (antiparticle) and X ($\bar{X}$) is a SM (or any of its extension) visible particle (antiparticle). This process acted during an early epoch and afterwards χ was "frozen out" because of roughly speaking too fast Universe expansion relative to the interaction rate. This chapter is about this phenomenology, see [1] (chapter 5), and for a brief review [2] (chapter 3) and [3].

Let us consider any species in the Universe which is in thermodynamic equilibrium with itself.

In our case it will be just WIMP. But it may also be for example cosmic background radiation (CMB) as well. It may be described using a distribution function $f(p^\mu, x^\mu)$ (where x and p are respectively coordinates and momenta of the particles) and the relativistic Boltzmann equation

$$Lf = Cf, \tag{1.9}$$

where

$$L = p^\alpha \frac{\partial}{\partial x^\alpha} - \Gamma^\alpha_{\beta\gamma} p^\beta p^\gamma \frac{\partial}{\partial p^\alpha}, \tag{1.10}$$

and C is an interaction which will be discussed below. For the FRW model (Friedman-Robertson-Walker model) f is spatially homogeneous $f = f(E,t)$ and using the metric properties

$$Lf(E,t) = E\frac{\partial f}{\partial t} - H(E^2 - m^2)\frac{\partial f}{\partial E} \ , \tag{1.11}$$

where

$$H = \frac{\dot{R}}{R} \ , \tag{1.12}$$

is the Hubble parameter, and R is the Universe radius.

The number density is

$$n(t) = \frac{g}{(2\pi)^3}\int d^3p f(E,t) \ , \tag{1.13}$$

where g counts internal degrees of freedom. After the integration over d^3p of (1.9) with (1.11) and multiplication by $\frac{g}{(2\pi)^3 E}$ one will have

$$\begin{aligned}
&\frac{g}{(2\pi)^3}\int d^3p \left[\frac{\partial f}{\partial t} - H\frac{(E^2-m^2)}{E}\frac{\partial f}{\partial E}\right] \\
=&\frac{\partial n}{\partial t} - \frac{gH4\pi}{(2\pi)^3}\int\limits_0^\infty dp \frac{p^2}{(p^2+m^2)^{\frac{1}{2}}} p^2 \frac{\partial p}{\partial E}\frac{\partial f}{\partial p} \\
=&\frac{\partial n}{\partial t} - \frac{gH4\pi}{(2\pi)^3}\int\limits_0^\infty dp \frac{p^4}{(p^2+m^2)^{\frac{1}{2}}} \frac{(p^2+m^2)^{\frac{1}{2}}}{p}\frac{\partial f}{\partial p} \\
=&\frac{\partial n}{\partial t} - \frac{gH4\pi}{(2\pi)^3}\int\limits_0^\infty dp p^3 \frac{\partial f}{\partial p} \\
=&\frac{\partial n}{\partial t} + \frac{gH4\pi}{(2\pi)^3}\int\limits_0^\infty dp 3p^2 f \\
=&\frac{\partial n}{\partial t} + 3H\frac{g}{(2\pi)^3}\int\limits_0^\infty d^3p f \\
=&\frac{\partial n}{\partial t} + 3Hn \ .
\end{aligned} \tag{1.14}$$

The right-hand side of (1.9) describes a contribution of the process between different species

$$\chi + a + b + \cdots \leftrightarrow i + j + \cdots \ . \tag{1.15}$$

and it is after the integration

$$\begin{aligned} &\frac{g}{(2\pi)^3}\int d^3p_\chi C f(E_\chi) \\ &= -d\Pi_\chi d\Pi_a d\Pi_a ... d\Pi_i d\Pi_j ... (2\pi)^4\delta(p_\chi + p_a + p_b + ... - p_i - p_j - ...)\times \\ &\times \left[|M|^2_{\chi+a+b\to i+j+...} f_\chi f_a f_b ... (1 \pm f_i)(1 \pm f_j) ... - \right. \\ &\left. -|M|^2_{i+j+...\to\chi+a+b+...} f_i f_j ... (1 \pm f_\chi)(1 \pm f_a)(1 \pm f_b) ... \right] \ . \end{aligned} \tag{1.16}$$

Here, f_X is the phase space density of the X particle, $\pm$ is plus for bosons and minus for fermions, and

$$d\Pi \equiv \frac{g}{(2\pi)^3}\frac{d^3p}{2E} \ . \tag{1.17}$$

In principle, if any species interacts with any other strongly enough, besides the interaction that we are interested in, this group of species will have equilibrium phase space distribution function, reducing the problem to a single integral-partial-differential equation for the one species of interest.

We assume CP invariance of the key process (1.15) which leads to

$$|M|^2_{i+j+...\to\chi+a+b+...} = |M|^2_{\chi+a+b+...\to i+j+...} = |M|^2 \ . \tag{1.18}$$

Furthermore, we will assume Maxwell-Boltzmann statistics for all species. In the absence of Bose condensation or Fermi degeneracy $1 \pm f \approx 1$ and

$$f_X(E_X) = \exp\left[-(E_X - \mu_X)/T\right] \ , \tag{1.19}$$

where μ_X is the chemical potential of species X. So one has

$$\begin{aligned} &\dot{n}_\chi + 3Hn_\chi \\ &= -\int d\Pi_\chi d\Pi_a d\Pi_b ... d\Pi_i d\Pi_j ... (2\pi)^4\delta(p_\chi + p_a + p_b + ... - p_i - p_j - ...)\times \\ &\times |M|^2 \left[f_\chi f_a f_b ... - f_i f_j ...\right] \ . \end{aligned} \tag{1.20}$$

In the absence of any interaction ($M = 0$) n_χ will be defined by the expansion of the universe only: $n_\chi \sim R^{-3}$. In the contrary case when the universe expansion is negligible the system would just exponentially approach the state of thermodynamic equilibrium or simply be in the equilibrium. If the first case replaces the second during the history of the universe or in other words the universe begins to expand faster than the species interact the phase of equilibrium will be replaced by the phase with "frozen" χ species.

We suppose now that χ is stable. So we are interested in annihilation processes only. In our case of the first nontrivial perturbative order it will be just 2 to 2 processes

$$\bar{\chi} + \chi \leftrightarrow X + \bar{X} \ , \tag{1.21}$$

where X is any species into which χ can annihilate. We consider a case with not identical χ and $\bar{\chi}$ for generality,

$$\begin{aligned} &\dot{n}_\chi + 3Hn_\chi \\ &= -\int d\Pi_\chi d\Pi_{\bar{\chi}} d\Pi_X d\Pi_{\bar{X}} (2\pi)^4 \delta(p_\chi + p_{\bar{\chi}} - p_X - p_{\bar{X}}) |M|^2 \left[f_\chi f_{\bar{\chi}} - f_X f_{\bar{X}} \right] \ . \end{aligned} \tag{1.22}$$

We assume that there is no asymmetry between χ and $\bar{\chi}$. The next assumption is that

$$\begin{aligned} f_X &= c_X^{-1} \exp\left[-\frac{E_X}{T} \right], \ f_{\bar{X}} = c_{\bar{X}}^{-1} \exp\left[-\frac{E_{\bar{X}}}{T} \right], \\ f_\chi &= c_\chi^{-1} \exp\left[-\frac{E_\chi}{T} \right], \ f_{\bar{\chi}} = c_{\bar{\chi}}^{-1} \exp\left[-\frac{E_{\bar{\chi}}}{T} \right], \end{aligned} \tag{1.23}$$

which means that X, $\bar{X}$, χ and $\bar{\chi}$ are in thermal equilibrium and c_X, $c_{\bar{X}}$, c_χ, and $c_{\bar{\chi}}$ are proper T-dependent normalization coefficients. So

$$f_\chi f_{\bar{\chi}} = c_\chi^{-1} c_{\bar{\chi}}^{-1} \exp\left[-\frac{E_\chi + E_{\bar{\chi}}}{T} \right] \ , \tag{1.24}$$

$$f_X f_{\bar{X}} = c_X^{-1} c_{\bar{X}}^{-1} \exp\left[-\frac{E_X + E_{\bar{X}}}{T} \right] = c_X^{-1} c_{\bar{X}}^{-1} \exp\left[-\frac{E_\chi + E_{\bar{\chi}}}{T} \right] = f_\chi^{EQ} f_{\bar{\chi}}^{EQ} \ , \tag{1.25}$$

because of the energy conservation law $E_X + E_{\bar{X}} = E_\chi + E_{\bar{\chi}}$. Here f_χ^{EQ} and $f_{\bar{\chi}}^{EQ}$ are equilibrium values of the χ and $\bar{\chi}$ phase functions. So

$$\frac{n_\chi n_{\bar{\chi}}}{n_\chi^{EQ} n_{\bar{\chi}}^{EQ}} = \frac{\int d^3p_\chi d^3p_{\bar{\chi}} c_\chi^{-1} c_{\bar{\chi}}^{-1} \exp\left[-\frac{E_\chi + E_{\bar{\chi}}}{T} \right]}{\int d^3p_\chi d^3p_{\bar{\chi}} c_X^{-1} c_{\bar{X}}^{-1} \exp\left[-\frac{E_\chi + E_{\bar{\chi}}}{T} \right]} = \frac{c_\chi^{-1} c_{\bar{\chi}}^{-1}}{c_X^{-1} c_{\bar{X}}^{-1}} \tag{1.26}$$

and

$$\begin{aligned} &f_\chi f_{\bar{\chi}} - f_X f_{\bar{X}} = f_\chi f_{\bar{\chi}} - f_\chi^{EQ} f_{\bar{\chi}}^{EQ} = \exp\left[-\frac{E_\chi + E_{\bar{\chi}}}{T} \right] \left[1 - \frac{c_\chi^{-1} c_{\bar{\chi}}^{-1}}{c_X^{-1} c_{\bar{X}}^{-1}} \right] \\ &= \exp\left[-\frac{E_\chi + E_{\bar{\chi}}}{T} \right] \left[1 - \frac{n_\chi n_{\bar{\chi}}}{n_\chi^{EQ} n_{\bar{\chi}}^{EQ}} \right] \ . \end{aligned} \tag{1.27}$$

Following [1] let us define

$$\begin{aligned} &\langle \sigma_{\chi\bar{\chi}\to X\bar{X}} |v| \rangle \stackrel{\text{def}}{=} \\ &\stackrel{\text{def}}{=} (n_\chi^{EQ} n_{\bar{\chi}}^{EQ})^{-1} \\ &\cdot \int d\Pi_\chi d\Pi_{\bar{\chi}} d\Pi_X d\Pi_{\bar{X}} (2\pi)^4 \delta(p_\chi + p_{\bar{\chi}} - p_X - p_{\bar{X}}) |M|^2 \exp\left[-\frac{E_\chi + E_{\bar{\chi}}}{T} \right] \ , \end{aligned} \tag{1.28}$$

then

$$\dot{n}_\chi + 3Hn_\chi = -\langle\sigma_{\chi\bar{\chi}\to X\bar{X}}|v|\rangle\left[n_\chi n_{\bar{\chi}} - n_\chi^{EQ} n_{\bar{\chi}}^{EQ}\right] \ , \tag{1.29}$$

It is convenient to use the variable

$$Y = \frac{n_\chi}{s} \ , \tag{1.30}$$

where s is the entropy density, instead of n_χ. Due to the entropy conservation property $sR^3 = const$ one has

$$\dot{s}R = -3s\dot{R} \tag{1.31}$$

and

$$s\dot{Y} = \frac{\dot{n_\chi}s - n_\chi\dot{s}}{s} = \dot{n_\chi} + 3\frac{\dot{R}}{R}n_\chi = \dot{n_\chi} + 3Hn_\chi \ , \tag{1.32}$$

which is exactly the left-hand side of (1.38).

It will also be useful to introduce

$$x = \frac{m}{T} \ , \tag{1.33}$$

where m is a mass scale, for example the mass of χ, instead of time t because the interaction depends upon temperature rather than time.

During the history of the Universe as the temperature decreases the number of effective degrees of freedom g_* decreases too. Fig. 1.6 illustrates this dynamics.

In the early Universe epoch which is a time of radiation domination [1]

$$H = \frac{g_*^{\frac{1}{2}}T^2}{2cm_{Pl}} = x^{-2}H(m) \ , \tag{1.34}$$

$$H(m) = \frac{g_*^{\frac{1}{2}}m^2}{2cm_{Pl}} \ , \tag{1.35}$$

where $c \approx 0.301$, g_* is an effective number of degrees of freedom [1], and $m_{Pl} = 1.22 \cdot 10^{19}$ GeV is the Planck mass, H is still a Hubble parameter and $H(m)$ is mass dependent Hubble parameter (terminology from [1]). Furthermore [1]

$$t = cg_*^{-\frac{1}{2}}\frac{m_{Pl}}{T^2} = \frac{cg_*^{-\frac{1}{2}}m_{Pl}x^2}{m^2} \ , \tag{1.36}$$

where t is time. So

$$\dot{Y} = -\frac{dY}{dx}\frac{m^2}{2cg_*^{-\frac{1}{2}}m_{Pl}x} = -\frac{dY}{dx}\frac{H(m)}{x} \ . \tag{1.37}$$

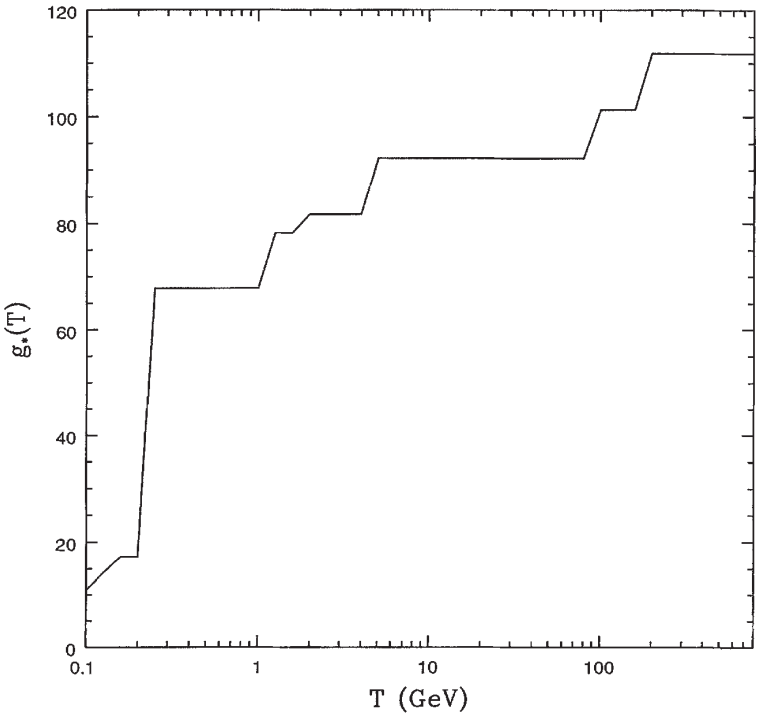

Figure 1.6: The number of effective relativistic degrees of freedom, g_* as a function of temperature. From [2].

So the Boltzmann equation can be rewritten as

$$\frac{dY}{dx} = -\frac{xs\langle\sigma_{\chi\bar{\chi}\to X\bar{X}}|v|\rangle}{H(m)}\left[Y_\chi Y_{\bar{\chi}} - Y_\chi^{EQ} Y_{\bar{\chi}}^{EQ}\right] \ . \tag{1.38}$$

Summing over all annihilation channels one will have $\langle\sigma_A|v|\rangle$ and

$$\frac{dY}{dx} = -\frac{xs\langle\sigma_A|v|\rangle}{H(m)}\left[Y_\chi Y_{\bar{\chi}} - Y_\chi^{EQ} Y_{\bar{\chi}}^{EQ}\right] \ . \tag{1.39}$$

We assume now that there is no asymmetry between χ and $\bar{\chi}$:

$$\begin{aligned} Y_\chi &= Y_{\bar{\chi}} \\ Y_\chi^{EQ} &= Y_{\bar{\chi}}^{EQ} \ . \end{aligned} \tag{1.40}$$

Dividing (1.39) by Y_χ^{EQ} one has

$$\frac{x}{Y^{EQ}}\frac{dY}{dx} = -\frac{x^2 n^{EQ}\langle\sigma_A|v|\rangle}{H(m)}\left[\left(\frac{Y}{Y^{EQ}}\right)^2 - 1\right] \ . \tag{1.41}$$

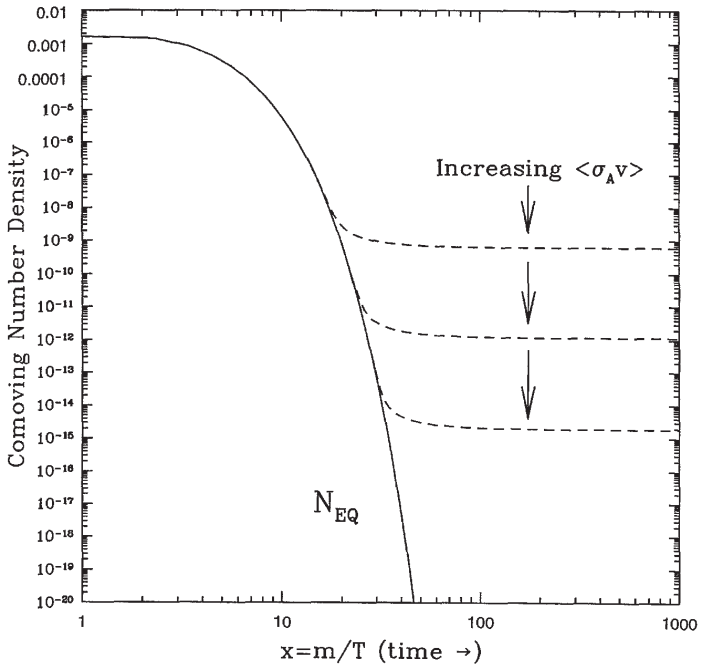

Figure 1.7: Comoving number density of a WIMP in the early Universe. The dashed curves the are actual abundance, and the solid curve is the equilibrium abundance. From [1] and [2].

Let

$$\Gamma_A = n^{EQ}\langle\sigma_A|v|\rangle \ . \tag{1.42}$$

So (see eq. (1.34))

$$\frac{x}{Y^{EQ}}\frac{dY}{dx} = -\frac{\Gamma_A}{H}\left[\left(\frac{Y}{Y^{EQ}}\right)^2 - 1\right] \ , \tag{1.43}$$

It is easy to see that the ratio $\frac{\Gamma_A}{H}$ defines what process is faster, the interaction Γ_A or the expansion H.

1.5.2 Solution of the Boltzmann equation

Let us consider first the case of energy independent $\langle\sigma_A|v|\rangle$ for the purpose of illustration.

In the early Universe $H \propto T^2$ (see eq. (1.34)) so the ratio $\frac{\Gamma_A}{H}$ is large and the interaction term dominates, number density tracks its equilibrium abundance, at later times after the fast expansion comoving abundance of χ's remains unchanged, see fig.1.7. The

characteristic temperature T_f of freeze-out is given by the equation

$$H(T_f) = \Gamma(T_f). \tag{1.44}$$

And for typical weak-scale numbers it turns out that $T_f = c_f m_\chi$, for $c_f \simeq \frac{1}{20}$ (see [2]). So the particles are *mostly* moving with nonrelativistic velocities when they freeze out.

We suppose that the entropy per comoving volume in the Universe remains constant as well as n_χ, so n_f/s remains constant as well. In accordance with [2]

$$s = c_s g_* T^3 \ , \tag{1.45}$$

where $c_s \simeq 0.4$. Using (1.34) and (1.44) one can find

$$\begin{aligned} &\left.\frac{n_\chi}{s}\right|_{\text{now}} = \left.\frac{n_\chi}{s}\right|_{\text{freeze-out}} \\ =&\frac{H}{c_s g_* T^3 \langle\sigma_A|v|\rangle} = \frac{g_*^{\frac{1}{2}} T^2}{c_s g_* T^3 \langle\sigma_A|v|\rangle 2cm_{\text{Pl}}} = \frac{1}{2cc_s g_*^{\frac{1}{2}} m_{\text{Pl}} T \langle\sigma_A|v|\rangle} \\ =&\frac{1}{2cc_s c_f g_*^{\frac{1}{2}} m_{\text{Pl}} m_\chi \langle\sigma_A|v|\rangle} = \frac{c_{n/s}}{m_{\text{Pl}} m_\chi \langle\sigma_A|v|\rangle} \ , \end{aligned} \tag{1.46}$$

with $c_{n/s} \simeq 100$. Using that now $s_0 \simeq 4000$ cm^{-3} and $\rho_c \simeq 10^5 h^2$ GeV, one can find

$$\Omega_\chi h^2 = \frac{\rho_\chi}{\rho_c} h^2 = \frac{m_\chi n_\chi}{\rho_c} h^2 = \frac{m_\chi c_{n/s}}{\rho_c m_{\text{Pl}} m_\chi \langle\sigma_A|v|\rangle} h^2 = \frac{c_\Omega}{\langle\sigma_A|v|\rangle} \ , \tag{1.47}$$

with $c_\Omega = 3 \cdot 10^{-27} \text{cm}^3 \text{s}^{-1}$.

In this approximation the DM abundance is independent of the mass of the WIMP and defined by $\langle\sigma_A|v|\rangle$ only. As the annihilation cross section increases the WIMPs stay in equilibrium longer, and we are left with a smaller relic abundance.

The partial-wave unitarity of the S-matrix means [62]

$$\langle\sigma_A|v|\rangle \approx \frac{1}{m^2_{\text{WIMP}}} \ , \tag{1.48}$$

which leads to $M_{\text{WIMP}} \leq 340$ TeV (WMAP data gives $M_{\text{WIMP}} \leq 120$ TeV [3]).

In some cases, as for example if the annihilation occurs through a resonance in the s-channel (which is the case of the model considered in this text) the cross section can not be considered as constant. Although the freeze-out occurs for nonrelativistic velocities part of the DM particles move fast in accordance with the Maxwell distribution which may seriously deform the solution. Naive calculation as above leads to errors by a factor of two or more. Nevertheless (1.47) may be used for estimation and for qualitative analysis.

The microMEGAs software is able to calculate DM relic density by freeze-out approximation as well as by Runge-Kutta method for (1.38). The second way requires much machine time which is one of the technical problems.

Chapter 2

Two Higgs Doublets plus 1 Singlet

2.1 General structure of the two Higgs doublet model

In the general case the Two-Higgs-Doublet Model (2HDM) is just the SM with two Higgs doublets instead of one. Such models are described in [63, 64, 65, 66, 67, 68, 69, 70, 71]. This is a very brief review of the model structure.

The 2HDM can be seen as just an unconstrained version of the Higgs sector of the MSSM.

In the general case the Higgs interaction sector in terms of doublet fields ϕ_1 and ϕ_2 is given by the potential

$$\begin{aligned} V_{\text{doublet}}(\phi_1,\phi_2) = &-\frac{1}{2}m_{11}^2\phi_1^+\phi_1 - \frac{1}{2}m_{22}^2\phi_2^+\phi_2 - \left[\frac{1}{2}m_{12}^2\phi_1^+\phi_2 + H.c.\right] + \\ &+\frac{1}{2}\lambda_1\left(\phi_1^+\phi_1\right)^2 + \frac{1}{2}\lambda_2\left(\phi_2^+\phi_2\right)^2 + \lambda_3\left(\phi_1^+\phi_1\right)\left(\phi_2^+\phi_2\right) + \lambda_4\left(\phi_1^+\phi_2\right)\left(\phi_2^+\phi_1\right) + \\ &+\frac{1}{2}\left[\lambda_5\left(\phi_1^+\phi_2\right)^2 + H.c.\right] + \\ &+\frac{1}{2}\left[\lambda_6(\phi_1^+\phi_1)(\phi_1^+\phi_2) + H.c.\right] + \frac{1}{2}\left[\lambda_7(\phi_2^+\phi_2)(\phi_1^+\phi_2) + H.c.\right] , \end{aligned} \tag{2.1}$$

where the parameters $m_{12}\,, \lambda_5\,, \lambda_6\,, \lambda_7$ can be complex and all other parameters are real because of the hermiticity requirement.

After the gauge symmetry is spontaneously broken, the doublet fields can be represented as

$$\phi_i = \begin{pmatrix} \phi_i^+ \\ \frac{1}{\sqrt{2}}\left(v_i + \eta_i + i\chi_i\right) \end{pmatrix} , \tag{2.2}$$

$$\tan\beta = \frac{v_2}{v_1} . \tag{2.3}$$

Two complex doublets with $SU(2) \times U(1)$ broken to the $U(1)$ gauge group generate one electrically charged ($H^{\pm}$) and three neutral ($H_i,\ i = 1, 2, 3$) massive Higgs particles instead of one neutral Higgs boson in the SM. There are also the usual Goldstone boson degrees of freedom G^0 and G^+. It is convenient to define

$$\eta_3 = -\sin\beta\chi_1 + \cos\beta\chi_2\,, \tag{2.4}$$

$$H_j = R_{ji}\eta_i\,, \tag{2.5}$$

$$H^+ = -\sin\beta\phi_1^+ + \cos\beta\phi_2^+\,, \tag{2.6}$$

$$G^0 = \cos\beta\chi_1 + \sin\beta\chi_2\,, \tag{2.7}$$

$$G^+ = \cos\beta\phi_1 + \sin\beta\phi_2\,. \tag{2.8}$$

Here, R_{ji} is a rotation matrix which can be expressed as a function of m's and λ's. It can also be parametrized through rotation angles α_1, α_2 and α_3:

$$R = \begin{pmatrix} c_1c_2 & s_1c_2 & s_2 \\ -c_1s_2s_3 - s_1c_3 & c_1c_3 - s_1s_2s_3 & c_2s_3 \\ -c_1s_2c_3 + s_1s_3 & -c_1s_3 - s_1s_2c_3 & c_2c_3 \end{pmatrix}\,, \tag{2.9}$$

where

$$c_i = \cos\alpha_i\,, s_i = \sin\alpha_i\,. \tag{2.10}$$

Masses of the Higgs bosons ($M_1 \le M_2 \le M_3,\ M_{H^\pm}$) are also functions of m's and λ's as well as the parameters

$$v^2 = v_1^2 + v_2^2\ , \tag{2.11}$$

$$\nu = \mathrm{Re}\, m_{12}^2/(2v_1v_2)\ , \tag{2.12}$$

$$\mu^2 = v^2\nu\ . \tag{2.13}$$

We will be interested in the case of $\lambda_6 = \lambda_7 = 0$.

So instead of m's and λ's we have a set of parameters, which is more convenient for our purpose

$$v\,, \tan\beta\,, \mu\,, M_1\,, M_2\,, M_3\,, M_{H^\pm}\,, \alpha_1\,, \alpha_2\,, \alpha_3\ , \tag{2.14}$$

which is overcomplete, one parameter can be excluded. It will be convenient to remove M_3:

$$M_3^2 = \frac{M_1^2 R_{13}\left(-R_{11} + R_{12}\tan\beta\right) + M_2^2 R_{23}\left(-R_{21} + R_{22}\tan\beta\right)}{R_{33}\left(R_{31} - R_{32}\tan\beta\right)} \tag{2.15}$$

(see [72]). The parameter v is fixed from experiment like in the SM

$$v = 246 \text{ GeV} . \tag{2.16}$$

So 8 parameters remain free at this step of the investigation.

2.2 2HDM + 1 Singlet

We will introduce an extra singlet ϕ which is a dark matter candidate:

$$V_{\text{singlet}} = \mu_\phi^2\phi^2 + \frac{1}{4!}\lambda_\phi^4 + \phi^2\left(\eta_1\phi_1^+\phi_1 + \eta_2\phi_2^+\phi_2\right) . \tag{2.17}$$

This singlet is unbroken ($\mu_\phi^2 > 0$). So the mass of the particle is

$$m_\phi^2 = 2\mu_\phi^2 + \eta_1 v_1^2 + \eta_2 v_2^2 . \tag{2.18}$$

One can get the interaction in terms of physical fields [63]

$$V_{\text{singlet}} = \phi^2(\kappa_i v H_i + \lambda_{ij} H_i H_j + \lambda_\pm H^+ H^-) , \tag{2.19}$$

with

$$\kappa_i = \eta_1 R_{i1} c_\beta + \eta_2 R_{i2} s_\beta \tag{2.20}$$

$$\lambda_{ij} = \frac{1}{2}\left[\eta_1(R_{i1}R_{j1} + s_\beta^2 R_{i3}R_{j3}) + \eta_2(R_{i2}R_{j2} + c_\beta^2 R_{i3}R_{j3})\right] , \tag{2.21}$$

$$\lambda_\pm = \eta_1 s_\beta^2 + \eta_2 c_\beta^2 . \tag{2.22}$$

The singlet sector can be parametrized using 4 parameters:

$$M_\phi , \lambda_\phi , \eta_1 , \eta_2 . \tag{2.23}$$

We will suppose for simplicity that

$$\eta_1 = \eta_2 = \eta \tag{2.24}$$

2.3 Quadratic divergence cancellation in the 2HDM+1S

Quadratic divergence cancellation are discussed in [80, 81, 63]. It is an extra requirement for the theory which leads to fixing two of the parameters that were left arbitrary before. Both versions of the 2HDM+1S (constrained and unconstrained) will be discussed. In chapter 3 only the unconstrained case will be considered. Chapter 4 is about both versions.

The cancellation for the DM singlet particle ϕ requires the presence of fermions in the theory that can interact with ϕ because boson and fermion one-loop contributions to mass corrections are always with opposite sign. In [63] these fermions are right-handed neutrinos:

$$\mathcal{L}_Y = -\varphi\overline{(\nu_R)^c}Y_\varphi\nu_R + \text{H.c.}\ , \tag{2.25}$$

where Y_φ is a matrix.

The full set of equations is for the present case of 2HDM + 1S [63]

$$\begin{aligned}
\frac{3}{2}m_W^2 + \frac{3}{4}m_Z^2 + \frac{v^2}{2}\left(\frac{1}{2}\eta_1 + \frac{3}{2}\lambda_1 + \lambda_3 + \frac{1}{2}\lambda_4\right) &= 3\frac{m_b^2}{c_\beta^2}, \\
\frac{3}{2}m_W^2 + \frac{3}{4}m_Z^2 + \frac{v^2}{2}\left(\frac{1}{2}\eta_2 + \frac{3}{2}\lambda_2 + \lambda_3 + \frac{1}{2}\lambda_4\right) &= 3\frac{m_t^2}{s_\beta^2}, \\
\frac{\lambda_\varphi}{2} + 4(\eta_1 + \eta_2) &= 8\text{Tr}\{Y_\varphi Y_\varphi^\dagger\}.
\end{aligned} \tag{2.26}$$

The first two equations guarantee the cancellation in the doublet sector and the last one is for DM singlet mass.

The first two equations can be satisfied by fixing M_1 and M_2 (usually they are in the region from 100 GeV to 600 GeV as well as M_3). So these parameters are fixed and we have only 3 instead of 5 doublet parameters, they are μ, $\tan\beta$ and $M^\pm$.

2.4 Constraints

Because of natural physical requirements such as positivity, unitarity and perturbativity there are some restrictions for the parameters.

2.4.1 General theoretical restrictions

First of all, all squares of masses must be positive (they must also be larger then experimental limits but it will be discussed later). In particular, that means that (2.15) must give a value $M_3^2 > M_2^2$.

1. **Positivity or classical potential stability**

These restrictions for the 2HDM are known from [73]:

$$\begin{aligned} &\lambda_1, \lambda_2 > 0 \ , \\ &\lambda_3 > \sqrt{\lambda_1, \lambda_2} \\ &\lambda_L = \lambda_3 + \lambda_4 - |\lambda_5| > \sqrt{\lambda_1, \lambda_2} \ , \end{aligned} \tag{2.27}$$

there are also conditions from the singlet sector

$$\lambda_\phi, \eta_1, \eta_2 > 0 \ . \tag{2.28}$$

Roughly speaking λ_1,λ_2 and λ_3 must be positive and λ_3 and λ_4 must be sufficiently large.

2. **Unitarity**

   Tree-level unitarity requirements on the Higgs-Higgs-scattering sector for the 2HDM are formulated in [74]:

$$\begin{aligned} \Lambda^{\text{even}}_{21\pm} &= \frac{1}{2}\left(\lambda_1 + \lambda_2 \pm \sqrt{(\lambda_1 - \lambda_2)^2 + 4|\lambda_5|^2}\right) \ , \\ \Lambda^{\text{even}}_{01\pm} &= \frac{1}{2}\left(\lambda_1 + \lambda_2 \pm \sqrt{(\lambda_1 - \lambda_2)^2 + 4\lambda_4^2}\right) \ , \\ \Lambda^{\text{even}}_{00\pm} &= \frac{1}{2}\left(3(\lambda_1 + \lambda_2) \pm \sqrt{9(\lambda_1 - \lambda_2)^2 + 4(2\lambda_3 + \lambda_4)^2}\right) \ , \\ \Lambda^{\text{odd}}_{21} &= \lambda_3 + \lambda_4 \ , \\ \Lambda^{\text{odd}}_{20} &= \lambda_3 - \lambda_4 \ , \\ \Lambda^{\text{odd}}_{01\pm} &= \lambda_3 \pm |\lambda_5| \ , \\ \Lambda^{\text{odd}}_{00\pm} &= \lambda_3 + 2\lambda_4 \pm 3|\lambda_5| \ . \end{aligned} \tag{2.29}$$

$$|\Lambda^{Z_2}_{Y\sigma\pm}| < 8\pi \ . \tag{2.30}$$

   Roughly speaking all λ's may not be too large.

3. **Perturbativity**

   This means that the couplings can not be larger than of order unity.

2.4.2 Experimental constraints

These constraints are discussed in [69] for the general case of 2HDM and take into account only doublet sector parameters. The SM satisfies the constraints that will be discussed in this section quite well. But the contribution from extra particles can spoil the agreement. From an other side it may make some restrictions free, for example the lightest Higgs particle mass may be smaller than the one from the SM scenario (see point 1 from the next list).

1. $B - \bar{B}$ **oscillations.** This constraint excludes scenarios with small $\tan\beta$ (less than 1) or small $M^{\pm}$ (less than 400 GeV) [69].

2. $b \to s\gamma$**.** The restriction due to this branching ratio limits the mass and Yukawa couplings of the H^+. For the case of the 2HDM it is discussed in [77]. Because of this constraint fermion couplings must be sufficiently small.

3. **Higgs non-discovery at LEP.** The neutral Higgs boson is not discovered at LEP2. This excluded SM scenarios with mass less than 114.4 GeV but it is also possible that the particle interacts with the Z boson more weakly (as for example in the 2HDM) or it decays to final states that are more difficult to detect.

   So this constraint is not only for M_1, but also (alternatively) for the ZZH and $\bar{f}fH$ couplings. It restricts mostly $\tan\beta$ (not too large) and the rotation angles [69].

4. $\Delta\rho$**.** This constraint is discussed in [67] in detail. In SM the parameter

$$\rho = \frac{m_W^2}{m_Z^2 \cos^2\theta_W} \ , \tag{2.31}$$

   which is just 1 at tree level has loop corrections. The precise measurements are in striking agreement with the SM predictions. They are [78]

$$\rho = 1.0050 \pm 0.0010 \ . \tag{2.32}$$

   So there is a strong constraint on extended electroweak models. In the case of the 2HDM, roughly speaking, Higgs masses must not be too far from the gauge boson masses and not very much apart [69] (for the detailed analysis see the same paper).

5. **Muon anomalous magnetic moment** a_μ**.** This parameter [79]

$$a_{\mu\,\mathrm{exp}} = \frac{1}{2}(g-2)_{\mu\,\mathrm{exp}} = 11659208(5.4)(3.3) \times 10^{-10} \tag{2.33}$$

   is predicted by the SM with high accuracy. Two-loop corrections of the 2HDM may corrupt that. But in our case this constraint is negligible [69].

6. **Electron electric dipole moment.** It must be

$$|d_e| \lesssim 1 \times 10^{-27} [e\mathrm{cm}] \ . \tag{2.34}$$

   Two-loop effects from 2HDM may also violate this constraint.

Chapter 3

Allowed region in the (M_ϕ, η) plane

Using micrOMEGAs [82] which is a tool for DM studies it is possible to calculate Ω_{dark} in any extension of the SM, in particular the 2HDM+1S and compare it with WMAP data.

The purpose of this section is to find allowed areas in the parameter space that satisfy all model constraints which includes proper values for Ω_{dark}. It is done with a program written in fortran77 which is just a modification of the analogous one that was used in [64]. In this chapter only the unconstrained 2HDM+1S is discussed, i.e., no condition of quadratic divergence cancellation is imposed.

There will be two main difficulties:

1. The large number of parameters of the model:

   (a) 2HDM parameters: M_1,M_2,μ, $\tan\beta$,$M^{\pm}$, α_1,α_2 and α_3

   (b) Singlet parameters: M_ϕ,η_1,η_2. We will assume $\eta_1 = \eta_2 = \eta$

   So one has to draw a lot of composite plot series and/or fix some parameters arbitrary.

2. The procedure of Ω_{dark} calculation requires much machine time. So one has to draw histograms with low resolution and it will be necessary to find nontrivial methods (computer program algorithms) that limit the number of Ω_{dark} evaluations.

The second purpose of this thesis is also a drill of different methods of calculation optimization that allow to save machine time. These are very technical and are carried out in appendix A and B. They are not so informative as just drill of a new method.

3.1 Calculation method and parameters.

It is convenient for the investigation to divide all free parameters into 2 groups:

1. Fixed parameters, which are

   - M_ϕ=20,30,...120 GeV.

- $\eta = 0.1, 0.2, ...0.9$
- $M_1 = 100, 200, ..., 600$ GeV
- $M_2 = 100, 200, ..., 600$ GeV, and $M_1 \leq M_2$

2. Flexible (random) parameters, that means that they are will be put random for each value of the fixed parameters. These are

   - $\mu = 200...700$ GeV
   - $\log_{10} \tan\beta = -1...2$ ($\tan\beta = 0.1...100$),
   - $M^{\pm} = 200...700$ GeV,
   - $\alpha_i = -\pi/2... + \pi/2$, $i = 1, 2, 3$.

   The density of the probability to get the value of any parameter is homogeneous in this parameterisation.

So the program just selects the second group of parameters randomly. After that it goes over all possible values of the parameters from the first group, and check if the model with this combination of parameters satisfies all theoretical and experimental constraints that were discussed in sec. 2.4.

The result of this calculation in the form of $M_\phi \times \eta$ histograms with the allowed regions for the case when $M_1 = 300$ GeV and $M_2 = 400$ GeV is presented in fig. 3.1.

It should be remarked that the histogram consists of "squares" which means that a point in the *center* of them is "good". It means that there is (has been found) at least one combination of the other (from the second group) parameters such that the model satisfies all constraints. But the existence of a "square" does not means that all point in the square are allowed.

Before the comments and the explanation of this result let us discuss some properties of these calculations.

3.2 The problem of validity

The first problem is that there is a chance that not all allowed "squares" are found and the presented area on the histogram is smaller then the true one. It is the case when the allowed area in the space of the second group of parameters with fixed ones from the first group is very small and the probability to find even one good point is very small too.

In principle it is also possible that the allowed area in the (M_ϕ, η) histogram is not limited at all but the size of the allowed area in the random parameter space is just very small. So the question is:"*Is the allowed area limited or not.*" It is not easy to answer this question through analytical analysis of the model and theoretical and experimental constraints and it will not be attempted here. The numerical analysis is easier but by its very nature it can not give a complete answer. In the present thesis there will be three attempts (three methods) to give the numerical method answer: in sections 3.3, 3.5 and appendix B.

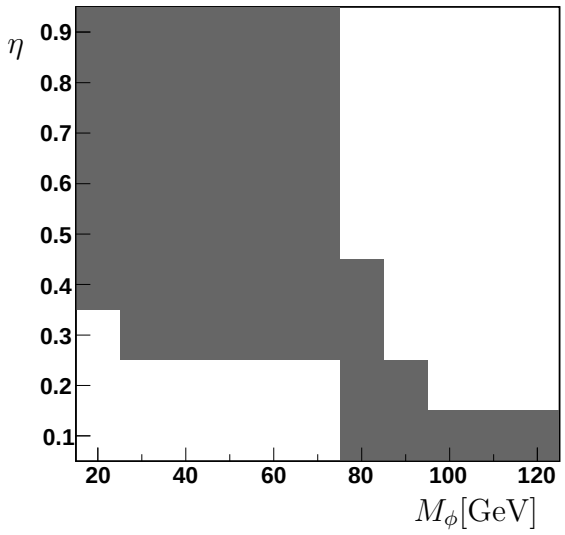

Figure 3.1: Allowed region (dark) histogram in the space of $M_\phi \times \eta$ for $M_1 = 300$ GeV, $M_2 = 400$ GeV.

3.3 Squares-attempts analysis

This subsection is to check the validity of the histograms in fig. 3.1 using the following analysis.

Let us consider the dependence of the number of found "squares" in the histograms and the number of attempts to find them (see fig. 3.2). As is easy to see the function grows slowly after about $10^{5.5}$ attempts. So it will be a good assumption that the function will not grow faster and not many new "squares" will be found.

This result can convince one that the result of this histogram in fig. 3.1 for such masses is valid and the area is limited (or at least there is a quality leap of the density function behavior (see sec. 3.5)).

3.4 Dependence on the $\Omega_{\mathbf{dark}}$ inaccuracy

To find the main reason which defines the form of the allowed areas let us change the inaccuracy of $\Omega_{\rm dark}$. This parameter is called $\sigma\Omega_{\rm dark}$. Increasing $\sigma\Omega_{\rm dark}$ makes the main experimental constraint softer (the allowed region is increased) and allows us to understand whether the boundary of the allowed areas is defined by the DM abundance or by any other reasons.

It will be studied in this section for the case of $M_1 = 300$ GeV and $M_2 = 400$ GeV (see

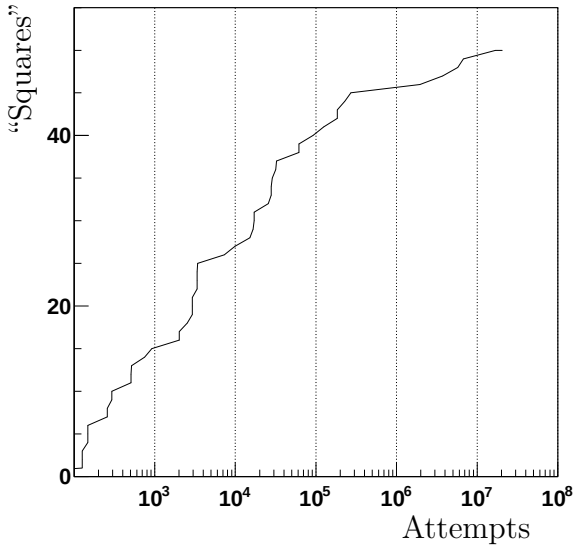

Figure 3.2: Dependence of the number of found allowed "squares" on the number of attempts in logarithmic scale for the case of $M_1 = 300$ GeV, $M_2 = 400$ GeV. It is visible that after about $10^{5.5}$ attempts not many new "squares" are found. It would be useful to make more attempts but it requires too much machine time.

fig. 3.3). It is clear that the boundary position is defined by $\sigma\Omega_{\text{dark}}$. But it is remarkable that the boundary near 80 GeV (see the scale in fig. 3.1) for large and medium η is quite stable (independent of the inaccuracy). It is because of the W-boson threshold in the DM annihilation channel (see sec. 3.6). Furthermore, as one can see, the third, fourth and fifth histograms are similar. The inaccuracy from the fifth histogram is $\sigma\Omega_{\text{dark}} \cdot 10^{+1} = 0.034$ which is about 30%. So the allowed region does not depend strongly on Ω_{dark}.

3.5 Boundary searching

This section is dedicated to attempts to explore the existence of a boundary and its precise value. For this purpose a mention of point density must be introduced.

Let us define density d as a ratio of the number of all found points for any value of the fixed parameters to the number of all attempts (checked random parameter combinations) to find them:

$$d = \frac{\text{number of found allowed points}}{\text{number of attempts}} \ . \tag{3.1}$$

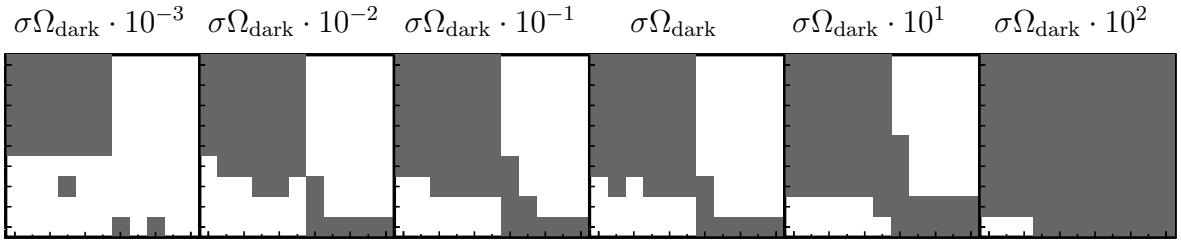

Figure 3.3: The same histograms as in fig. 3.1 but for different inaccuracies of $\Omega_{\rm dark}$ from $\sigma\Omega_{\rm dark} \to \sigma\Omega_{\rm dark} \cdot 10^{-3}$ (the left one) to $\sigma\Omega_{\rm dark} \to \sigma\Omega_{\rm dark} \cdot 10^{+2}$ (the right one). From left to right the $\sigma\Omega_{\rm dark}$ increases by a factor of 10 (see expressions under each histogram). The fourth histogram is with the actual $\sigma\Omega_{\rm dark}$, as in fig. 3.1.

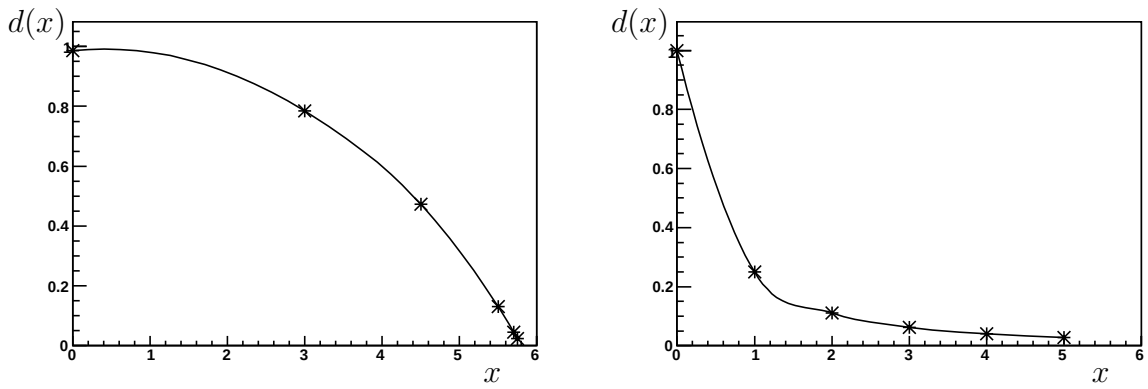

Figure 3.4: Two fictitious density functions. The horizontal axis corresponds to an argument x of these functions on which the function must be analysed if the boundary exists. On the left plot the function evidently tends to zero near $x \approx 5.8$ which is the boundary position. For the function on the right, it is not clear if a zero is reached.

This quantity reflects the probability to find an allowed point with given fixed parameters.

It may be useful to draw histograms with not only allowed regions but with a color that characterizes the density but it will not be done here. Instead the dependence of the density on M_ϕ and η will be used to explore the boundary existence of the allowed region.

In order to make two-dimensional plots it will be convenient to fix one parameter in the $M_\phi \times \eta$ space. Two quality types of the density dependence are possible (see fig. 3.4). The first one may be enough for someone to believe in the existence of a certain boundary of the region. Moreover it may allow us to calculate the boundary position with high accuracy. The second alternative may indicate that the boundary is absent or it is not easy to see it and determine its position.

The main technical difficulty is that the calculation of smaller values of d requires a large machine time because a lot of attempts are required.

This test was done for the case presented in fig. 3.1. Unfortunately such calculations (with fixed and random parameters defined as in sec. 3.1) requires much machine time and it was not possible to find many points for the graphs. But it will be much easier if one fixes some more parameters:

$$\begin{aligned} &M^{\pm} = 400 \text{ GeV}, \\ &\tan\beta = 1, \\ &\mu = 200 \text{ GeV}. \end{aligned} \tag{3.2}$$

So only the three α's are random. This assumption must not change the fact of boundary existence. The results for both choices of fixed and random parameters will be presented.

Two regions near the expected boundary in fig. 3.1 were tested in the above described way. The first one is near $M_\phi = 50$ GeV, $\eta \approx 4$, see fig. 3.5 with the density defined as in sec. 3.1 and fig. 3.6 with three fixed parameters. The second region is $\eta = 0.6$, $M_\phi \approx 75$ GeV. The analogous graphs are presented in figs. 3.7 and 3.8.

The results from the plots without extra parameter fixing are not very clear. But, as one can see, the pictures with fixed parameters is rather of the second type than of the first one (a boundary is visible). It is also possible to find the boundary position with high accuracy but it is not useful in the framework of the present investigation because the position strongly depends on $\sigma\Omega_{\text{dark}}$ (see discussion in sec 3.4).

The points (in this case mass M_ϕ for fixed η or η for fixed M_ϕ) for such graphs can be taken at equidistant point (for example $M_\phi = 70$ GeV, 80 GeV, 90 GeV...) or one can get them "by hand" such that they are concentrated near the expected boundary position in order to save calculation resources. The third alternative is to create a computer program that will finds an optimal way itself (automatic). Such program was developed and its algorithm is described in appendix A. All points from graphs in fig. 3.5, 3.6, 3.7 and 3.8 were found with this software.

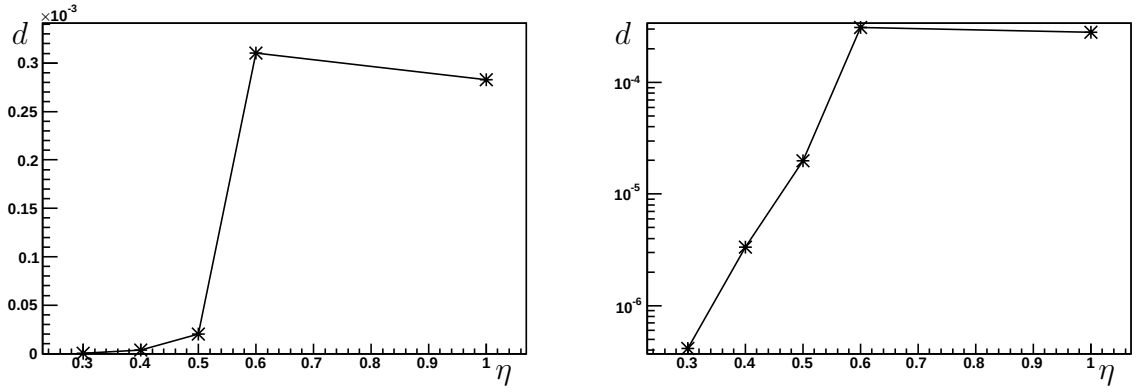

Figure 3.5: Density behavior for $M_\phi = 50$, $M_1 = 300$ GeV, $M_2 = 400$ GeV.

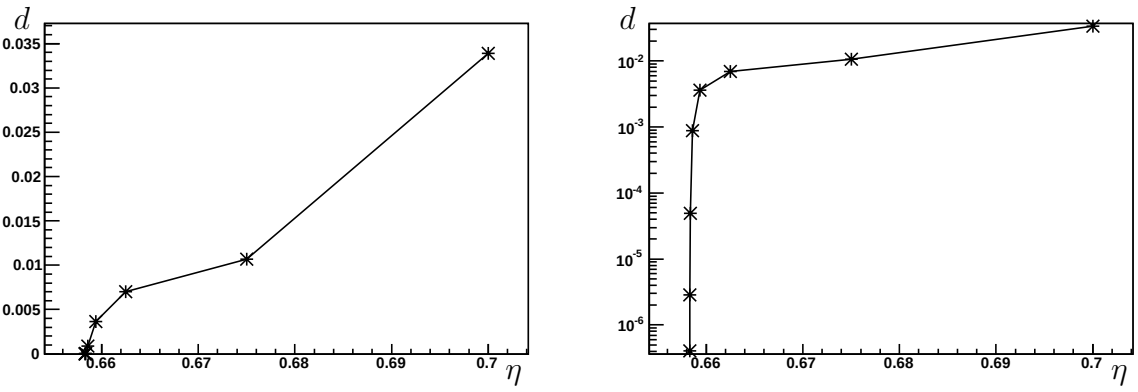

Figure 3.6: Density behavior for $M_\phi = 50$, $M_1 = 300$ GeV, $M_2 = 400$ GeV, $M^\pm = 400$ GeV, $\tan\beta = 1$, $\mu = 200$ GeV. A boundary does exist near $\eta = 0.658$.

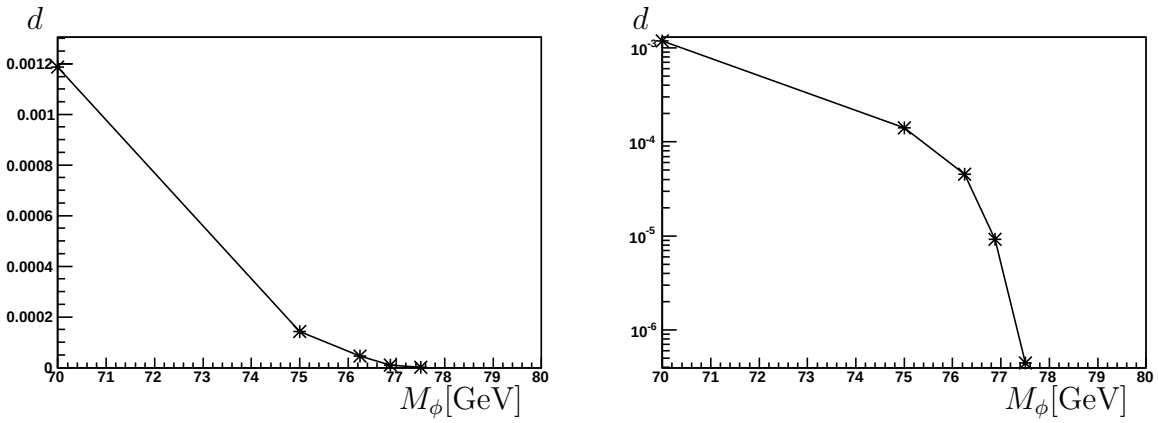

Figure 3.7: Density behavior for $\eta = 0.6$, $M_1 = 300$ GeV, $M_2 = 400$ GeV.

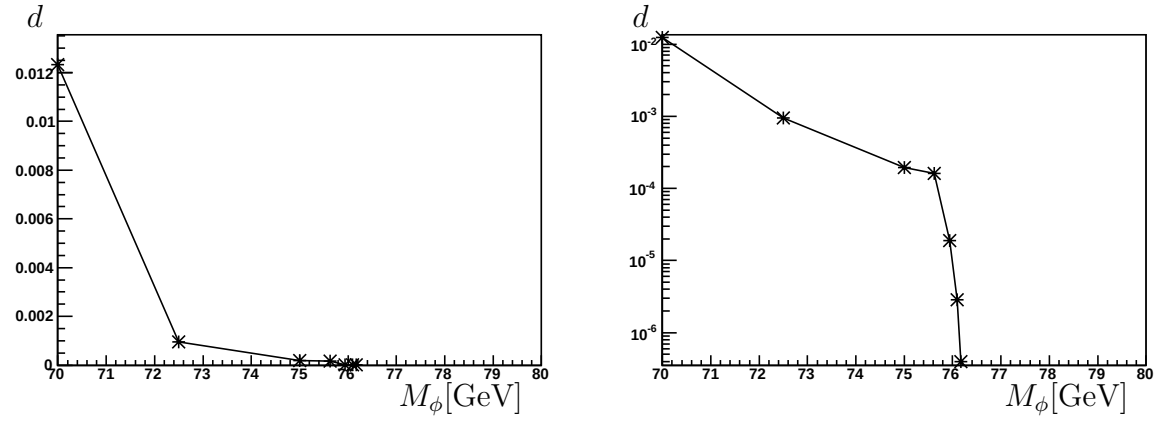

Figure 3.8: Density behavior for $\eta = 0.6$, $M_1 = 300$ GeV, $M_2 = 400$ GeV, $M^\pm = 400$ GeV, $\tan\beta = 1$, $\mu = 200$ GeV. A boundary does exist near $M_\phi = 76.2$ GeV.

3.6 Discussion of figure 3.1

In this chapter there will be an attempt to explain the results presented in fig. 3.1.

As in sec. 1.5 let us limit ourselves to $2 \to 2$ tree-level precesses. First of all there may be different products of the DM annihilation processes. Because of coldness of the DM ($E_\phi \approx M_\phi$) the possible products of the annihilation are limited by the DM particle mass M_ϕ. In GeV scale the important threshold is in W-boson mass because such channel is possible (and essential) only if $M_\phi \gtrsim M_W \approx 80$ GeV (symbol "$\gtrsim$" but not "$>$" is used because temperature Maxwell distribution allows a small probability of more heavy annihilation products).

One can see that the histogram (see fig. 3.1) can be separated into two parts: below and above 80 GeV. Allowed values of η are larger on the left side than on the right one. This is because beyond this threshold a new channel of annihilation is opened. It essentially contributes to the amplitude and the annihilation cross section is increased. To compensate that the coupling η has to be smaller which is observed in the histograms.

3.7 Results for different Higgs particle masses

The same result as in fig. 3.1 but for different values of M_1 and M_2 is presented in fig. 3.9.

Some of these histograms are not so clear-cut (see for example the cases $M_1 = 100$ GeV, $M_2 \geq 300$ GeV). So more attempts than are actually done are necessary. But it demands more and more machine time. Doing the same squares-attempts analysis as in sec. 3.3 one can see that indeed for these histograms the result does not seem to be complete. For example let us consider the case for $M_1 = 100$ GeV, $M_2 = 300$ GeV presented in fig. 3.10. The result confirms that the histogram is still not completed. On the other hand the same analysis for the case $M_1 = 600$ GeV, $M_2 = 600$ GeV presented in fig. 3.11 gives the opposite result that can convince one that the histogram is completed.

3.8 Analytic structure of DM annihilation cross section

In this section the approximate formula (1.47) will be used for qualitative analysis of the Ω_{dark} functional behavior. The cross section is defined by only s-channel resonance graph presented in fig. 3.12. So the cross section is proportional to

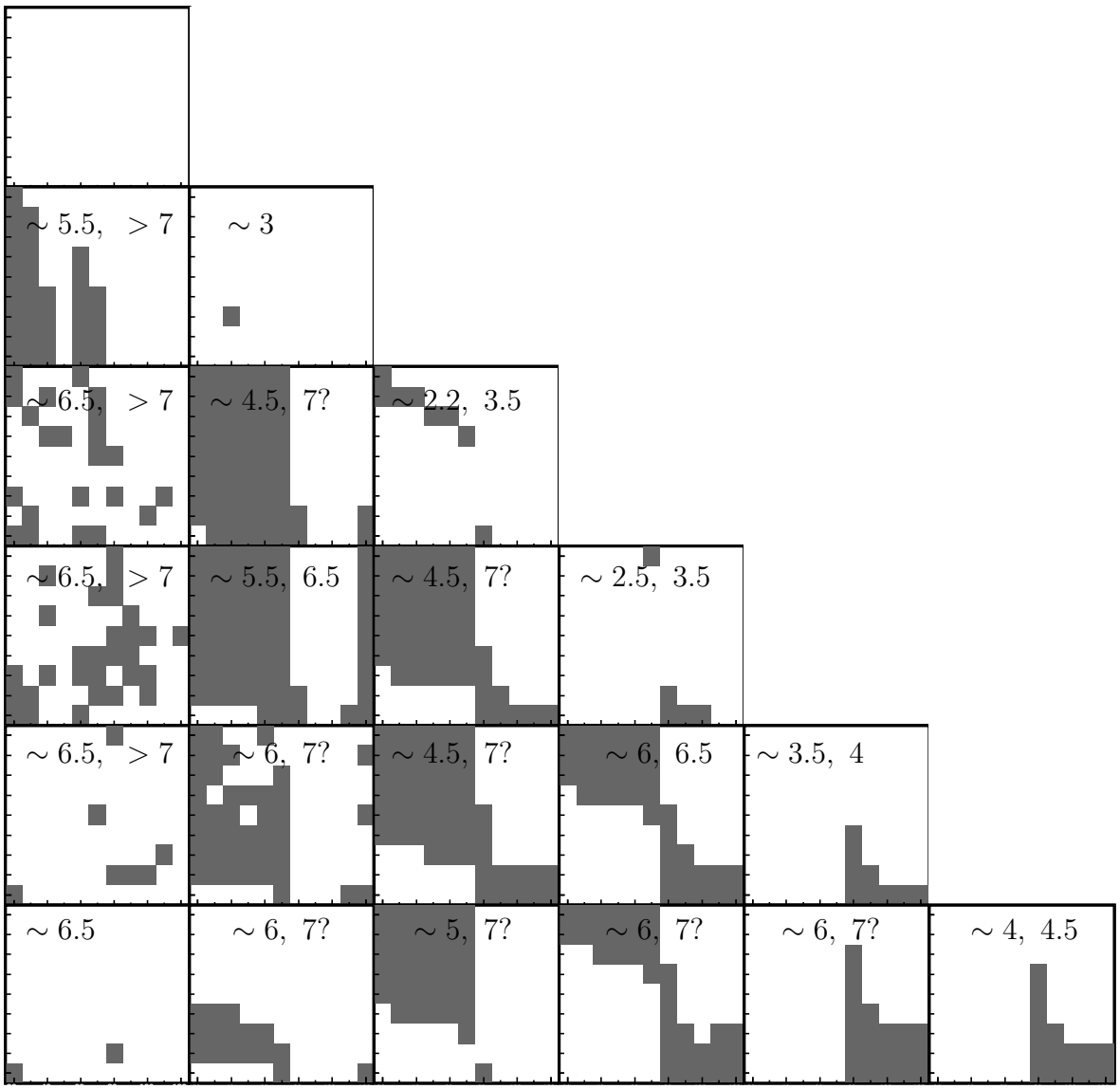

Figure 3.9: The same histograms as in fig. 3.1 but for different values of M_1 and M_2. The columns are with fixed M_1 from 100 GeV (the left column) to 600 GeV (the right column). The rows are with fixed M_2 from 100 GeV (the upper row) to 600 GeV (the bottom row). The numbers for each histogram indicate the validity of them. The first number is an order of number of attempts that were necessary to find the most part of the "squares". The second number is an order beyond which new "squares" were no longer found. "7?" means that it looks like to be completed but it is required more attempts to be sure. See the discussion in the text and comments for fig. 3.2, 3.10 and 3.11.

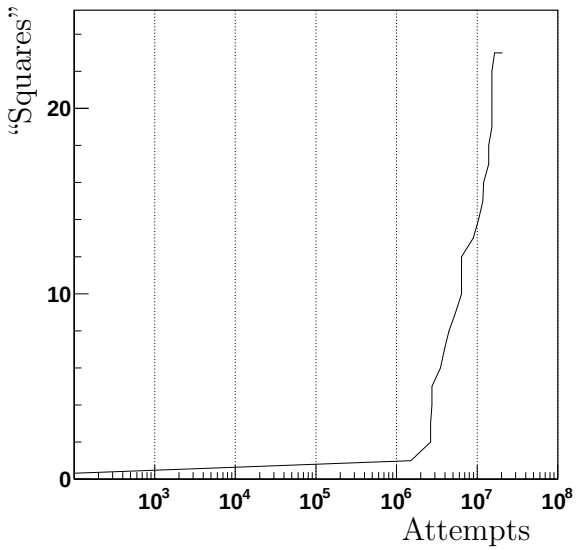

Figure 3.10: The dependence number of found allowed "squares" on the number of attempts in logarithmic scale for the case of $M_1 = 100$ GeV, $M_2 = 300$ GeV. The most part of "squares" is found only after about $10^{6.5}$ attempts. Most likely after more than 10^7 attempts many new "squares" will be found.

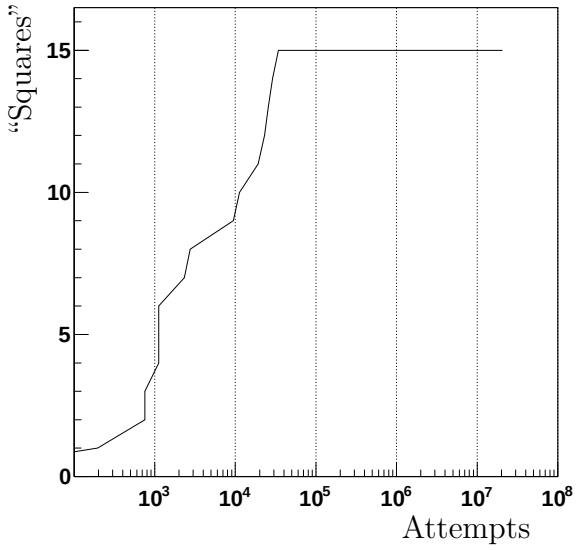

Figure 3.11: The dependence number of found allowed "squares" on the number of attempts in logarithmic scale for the case of $M_1 = 600$ GeV, $M_2 = 600$ GeV. Most likely all allowed points have been found and only about 10^4 attempt was required for that.

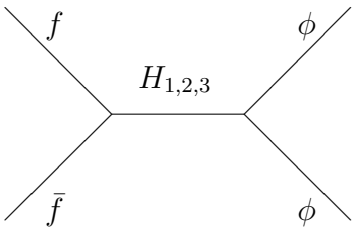

Figure 3.12: The only tree-level graph that contributes to DM annihilation cross section. Here, f and $\bar{f}$ are any 2HDM particles, fermions or gauge bosons, charged or neutral Higgs particles.

$$\sigma_A \sim \sum_{i=1,2,3} \left| \lambda_{Hf\bar{f}} \frac{1}{s - M_i^2} \lambda_{H\phi\phi} \right|^2 , \tag{3.3}$$

which for cold DM ($E_\phi \approx M_\phi$, $T \ll M_\phi$) gives

$$\langle \sigma_A |v| \rangle \sim \sum_{i=1,2,3} \left| \lambda_{Hf\bar{f}} \frac{1}{(2M_\phi)^2 - M_i^2} \lambda_{H\phi\phi} \right|^2 \sim \sum_{i=1,2,3} c_i \left| \lambda_{Hf\bar{f}} \frac{1}{2M_\phi - M_i} \lambda_{H\phi\phi} \right|^2 , \tag{3.4}$$

where c_i are some coefficients. This is not an exact formula, but it is true at the "qualitative level" and will be enough for the explanation. There are three factors:

1. $\lambda_{H\phi\phi}$, the singlet-sector coupling that is proportional to η,
2. $\lambda_{Hf\bar{f}}$, defined by the doublet-sector parameters,
3. $\frac{1}{2M_\phi - M_i}$, which depends on a neutral Higgs particle mass.

It clear from (3.4) that if $M_i \approx 2M_\phi$ the contribution to the cross section from the third factor (see above list) is very large which requires a low value of the product of singlet and doublet couplings.

Using the above facts one can explain some details of the histograms from fig. 3.9. For example a narrow hole near 50 GeV in the case of $M_1 = 100$ GeV, $M_2 = 200$ GeV is because it corresponds to the first Higgs particle. For $M_\phi = \frac{1}{2} M_1$ the third factor contribution is very large and only very small η is allowed. The same must be true for the other values of M_2.

Another consequence of the dependance on neutral Higgs masses is that with larger M_2 the allowed region before the threshold "moves up" (not allowed region with small η grows) and allowed region after the threshold grows to larger η too.

Chapter 4

Scatter plots

In contrast to the previous chapter, here another strategy of analysis is used. Instead of fixing some parameters, all of them will be random (in the second group) in certain intervals.

So the result is a large group of parameter combinations (points) that satisfy all constraints. This allows to draw scatter plots (2D or 3D) with any parameters along the axes using the same base of points.

This was done for the case of the (quadratic divergence cancellations) constrained model as well as for unconstrained.

4.1 The unconstrained model

As noted, all 10 parameters of the unconstrained model are random

- M_ϕ=20...120 GeV.
- $\eta = 0...1$
- $M_1 = 100...600$ GeV
- $M_2 = 100...600$ GeV, and $M_1 \leq M_2$
- $\mu = 200...700$ GeV
- $\log_{10} \tan\beta = -1...2$ ($\tan\beta = 0.1...100$),
- $M^\pm = 200...700$ GeV,
- $\alpha_i = -\pi/2... + \pi/2$, $i = 1, 2, 3$.

The result is shown in fig. 4.1. The upper left $M_\phi \times \eta$ panel results are in full accordance with the WW threshold discussion presented in sec. 3.6.

The situation for the other plots is not closely connected with the singlet sector and the DM constraint. It illustrates general properties of the 2HDM that are discussed (but

without such scatter plots histograms) in [69]. For example in the $\tan\beta \times M^{\pm}$ plot it is easy to see the constraints from B-physics for low $M^{\pm}$ and low $\tan\beta$ or the region with large $\tan\beta$ has not so many points because of the unitarity constraint.

4.2 The constrained model

As noted all 8 arbitrary parameters of the constrained model are now random

- M_{ϕ}=20...120 GeV.
- $\eta = 0...1$
- $\mu = 200...700$ GeV
- $\log_{10}\tan\beta = -1...2$ ($\tan\beta = 0.1...100$),
- $M^{\pm} = 200...700$ GeV,
- $\alpha_i = -\pi/2... + \pi/2$, $i = 1, 2, 3$.

The analogous to the result of the previous section is shown in fig. 4.2. It is similar to the previous one but there are some differences.

First of all the number of points in fig. 4.2 is smaller than in fig. 4.1 (because much machine time is required). On other hand the number of attempts to find them is larger in the constrained case. In other words the average density in the constrained case is lower. This is why there are many points for $\tan\beta > 10$ for the constrained case but not for the unconstrained one. If one will do the same number of attempts in the unconstrained case as in the second one will get the same result for $\tan\beta > 10$ but the region $\tan\beta \approx 1$ will be very dense.

The other visible detail is in the $\tan\beta \times M^{\pm}$ plot. All possible values of $\tan\beta$ are split into two groups: of $\tan\beta \approx 1$ (red points) and of $\tan\beta \approx 10..100$ (blue points). This separation does not affect the first histogram but for the red group of points it leads surely to smaller Higgs particle masses and large μ (see $M_1 \times M_2$ and $\mu \times M^{\pm}$ histograms). But it is actually a general property of the constrained 2HDM but not of the special 2HDM+1S case. Indeed the analogous scatter plots but without the constraint on $\Omega_{\rm dark}$ (WMAP data) are almost the same, except of course the $M_{\phi} \times \eta$ plot.

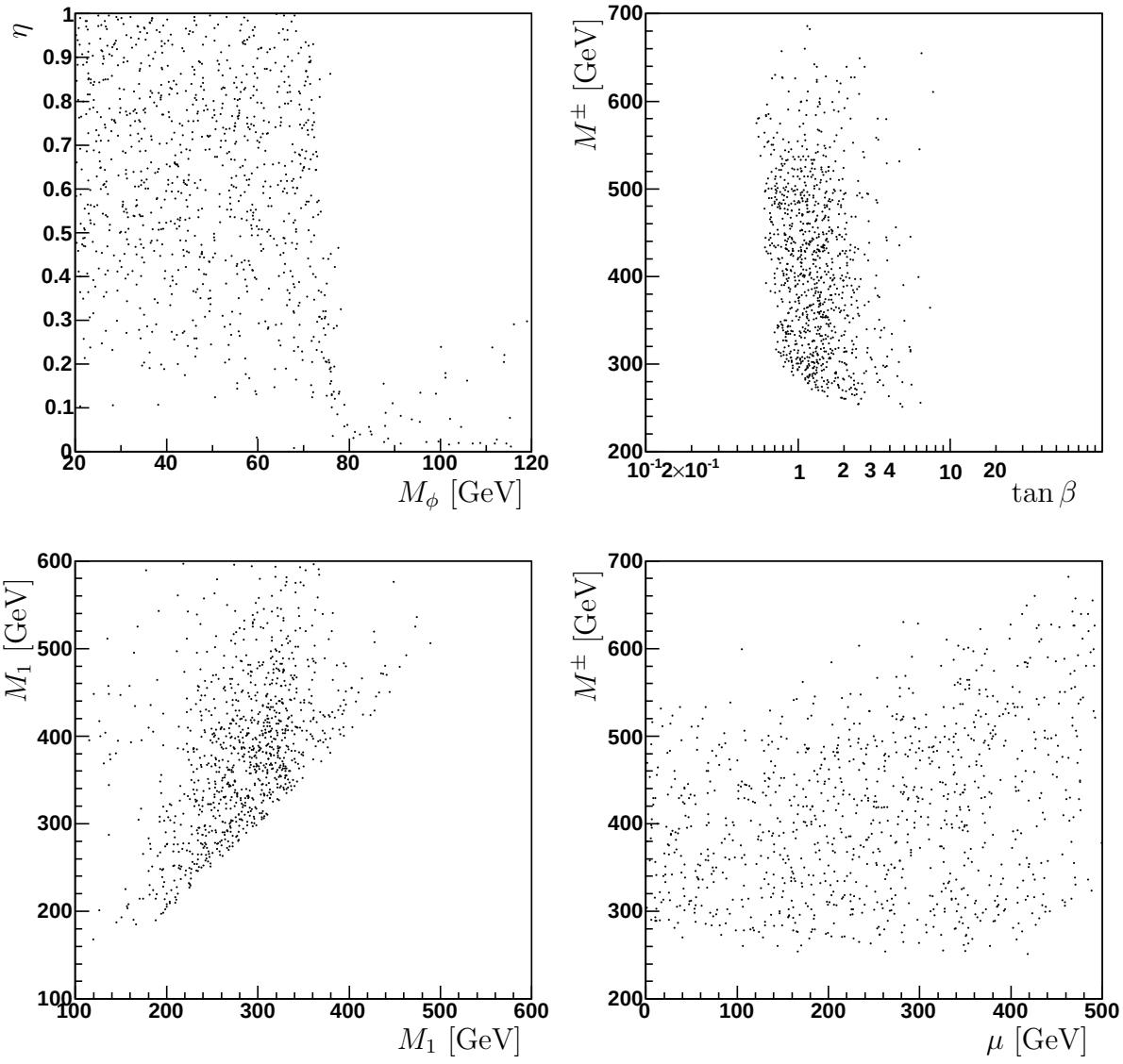

Figure 4.1: Scatter plots for the model without quadratic divergency cancellation. The left-top one is in $M_\phi \times \eta$ space like in histograms from chapter 3. The right-top one is in $\tan\beta \times M^\pm$ space, the lower left – $M_1 \times M_2$ and the lower right – $\mu \times M^\pm$.

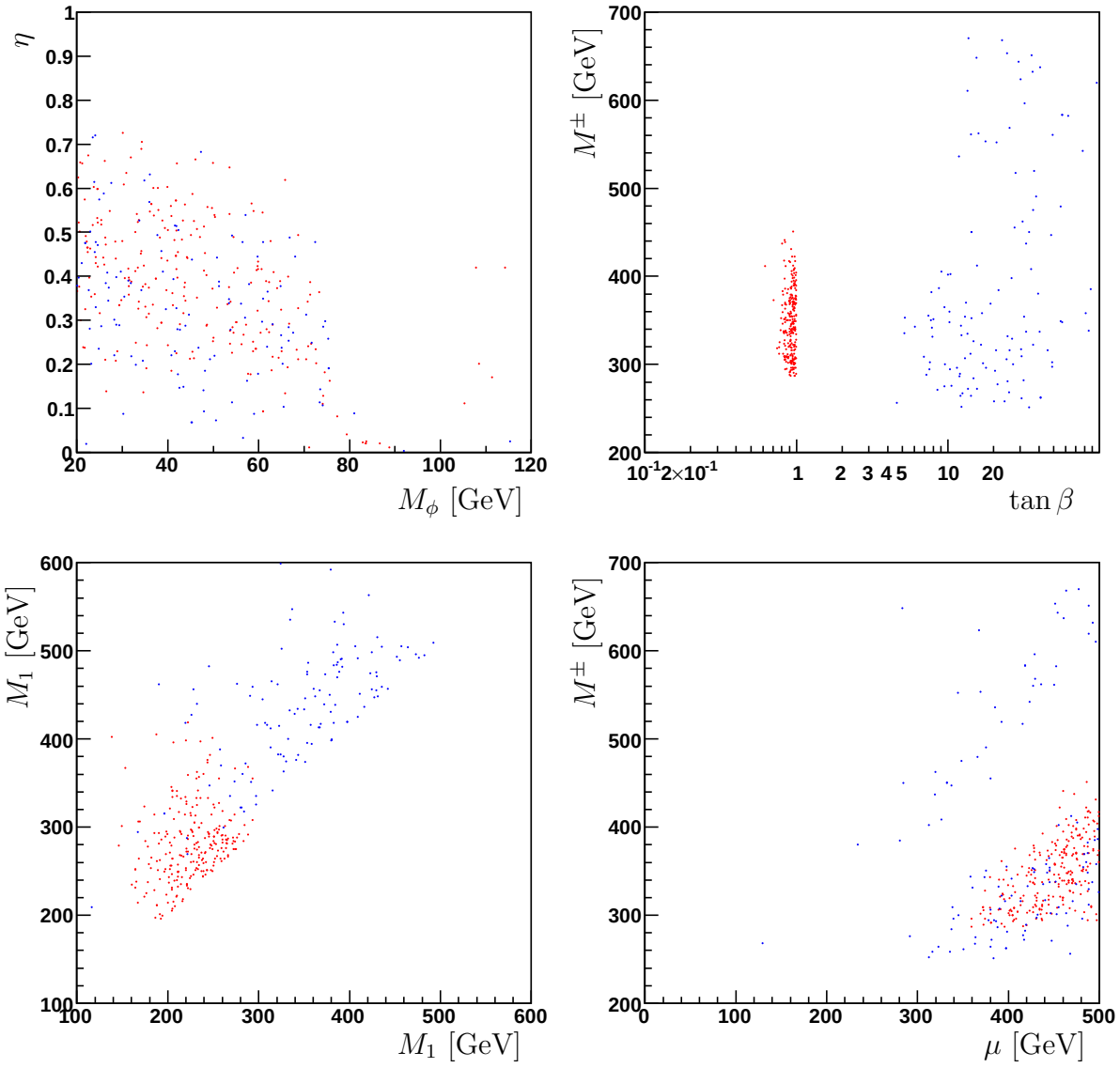

Figure 4.2: Scatter plots for the constrained model. The left-top one is in $M_\phi \times \eta$ space like in histograms from chapter 3. The right-top one is in $\tan\beta \times M^\pm$ space, the lower-left – $M_1 \times M_2$ and the lower-right – $\mu \times M^\pm$. All points are divided into two groups: the red ones are for small $\tan\beta$ (< 2) and the blue ones are for large $\tan\beta$ (> 2).

Summary

The 2HDM + 1S model has been explored as a theory with a DM particle. In both cases, with and without quadratic divergency cancellation constraints. WMAP data does not limit the parameters of the 2HDM+1S much. This constraint changes the allowed regions for the doublet parameters only very littele.

However the singlet parameters are limited, but allow any values of the DM particle mass in the explored region from 20 GeV to 120 GeV. It was found that the appropriate values of singlet parameters depend strongly on the Higgs particle masses (in the case of the unconstrained model) and this dependence was explored. It was also found that this allowed region of the singlet parameters does not strongly depend on the Ω_{dark} value (see sec. 3.4).

This result is in the agrement with the one from [64] (see fig. 5 in [64]), which was obtained with approximate formula (48) in [64] but not with more advanced methods such as micrOMEGAs.

Several different calculation methods such as "squares-attempts analysis" (see sec. 3.3) and "boundary searching" (see sec. 3.5) were used. These methods helped to analyze the result of direct search of allowed points in the parametric space. In particular the fact that the allowed region is limited was obtained. Furthermore they allow to estimate the validity of the results of numerical calculations (see sec. 3.2).

Some new numerical methods for the calculation of allowed regions were developed as algorithms, realized in fortran77 and tested (see appendix). They allow to someone to make an exact and economical calculation in any model, not only in the 2HDM+1S.

Appendix A

Algorithm for boundary calculation

This appendix is about a numerical calculation problem that arose in sec. 3.5. A new algorithm for automatic calculation and optimization was developed.

The general problem can be formulated as follows. Let there be a function $f(x, y)$, where x (y) is one or a set of arguments. The function is 1 or 0 ("good" or "bad" point (x, y)). We are interested in "good" areas for x, which means that for any y from Y there is at least one "good" point (x, y). The problem is that the f calculation requires much machine time. So the idea is to first define a density function $d(x)$ for any area Y for y

$$d(x) = \frac{\text{number of "good" points of } f(x,y) \text{ with } y \in Y}{\text{number of all points of } f(x,y) \text{ with } y \in Y} \ . \tag{A.1}$$

Of course the number of points in Y is actually infinite, but for the case of "good" functions f, $d(x)$ can be defined as a ratio of areas in parametric space for y. In our case there is no possibility to investigate f analytically but numerically only a finite number of points (x, y) can be calculated. So we suppose that f is "good" and calculate d numerically using a finite random set of points in Y. So $d(x) \geq 0$ and if it is 0 there is always a possibility that it is so small that just among the given finite number of all points no one happens to be "good".

The second point of the idea is to explore $d(x)$ in a region where it is very small and using any interpolation of the function it is possible first to find if the boundary of a "good" region exists or $d(x)$ just decreases asymptotically.

The direct calculation of $d(x)$ with any number of points in Y (10^N) for different values of x is too "wasteful". It is because for x with large d not many points are required and for regions with zero d it will not be useful to make so many attempts. Furthermore if it is necessary to find the boundary of the zero region with high accuracy it will require many points for x.

The present algorithm makes such calculation optimal and automatic. Let us suppose that $d(x)$ is a monotonically decreasing function from a point x. The idea is to do calculation in a region with large d with a small number of points (n) and move forward for larger values of x, increasing the n only if it allows to calculate nonzero $d(x)$ in this point. If it is not possible with current n (no point with current n have been found) one should

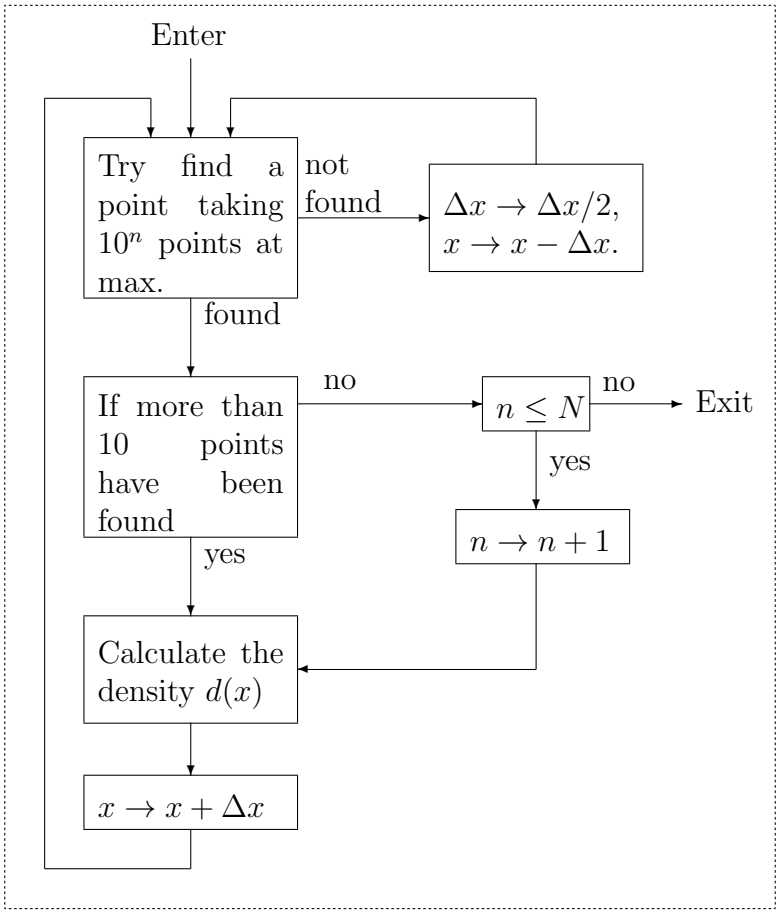

Figure A.1: Algorithm for boundary calculation.

move back a little and try to calculate $d(x)$ there. After that it is possible to return to the old points but with higher value of n. The algorithm is presented in fig. A.1.

The starting (input) data is N which specifies the maximal number of points (10^N) in Y that will be used. It is actually an accuracy of the boundary calculation that define the machine time that will be required. There is a starting point x, where the density is not zero (with a basic value n ($n < N$)) and basic step Δx. The result is a set of points x_i with $d(x_i)$ so that the points are concentrated near the boundary of zero region or at least near the area of small (of order 10^{-N}) $d(x)$.

The number 10 was used as a sufficiently big number of points for the calculation of $d(x)$ (the calculating was stopped after 10 "good" points have been found) (see the second from top left block in fig. A.1) and as a logarithmic "step" to increase the number of points. Someone can change this parameter if it is necessary.

A.1 Example

The algorithm was realized in fortran77 for the case of section 3.5. To illustrate how it works let us consider a case as in fig 3.8. The role of x is played by M_ϕ, the starting value is 70 GeV, $\Delta x = 10$ GeV. Starting $n = 4$. This is a protocol of the program (see also fig. 3.7 where the result point are presented in a form of graphic):

1. $M_\phi = 70$ GeV. The density is measured as $d = 1.2 \cdot 10^{-3}$. Move forward by 10 GeV.
2. $M_\phi = 80$ GeV. No point found with $n = 4$. Move backward by 5 GeV.
3. $M_\phi = 75$ GeV. The density is measured as $d = 1.4 \cdot 10^{-4}$. n was increased to $n = 5$ Move forward by 5 GeV.
4. $M_\phi = 80$ GeV. No point found with $n = 5$. Move backward by 2.5 GeV
5. $M_\phi = 77.5$ GeV. No point found with $n = 5$. Move backward by 1.25 GeV
6. $M_\phi = 76.25$ GeV. The density is measured as $d = 4.5 \cdot 10^{-5}$. n was increased to $n = 6$. Move forward by 5 GeV.
7. $M_\phi = 77.5$ GeV. No point found with $n = 6$. Move backward by 0.625 GeV.
8. $M_\phi = 76.25$ GeV. The density is measured as $d = 9.2 \cdot 10^{-6}$. n was increased to $n = 7$.
9. $M_\phi = 77.5$ GeV. The density is measured as $d = 4.4 \cdot 10^{-7}$. n was increased to $n = 8$. Move forward by 0.625 GeV.
10. ...

8 can be a maximal value ($N = 8$) or the calculation can continue.

The points for graphs in fig. 3.5, 3.6and 3.8 were calculated with this software in the same way.

So this method demonstrates that indeed the boundary exist. It may also be very effective if someone needed to find a boundary position with high accuracy.

Appendix B

Algorithm for quick "good" points search

This appendix is about a numerical calculation problem that arose in chapter 3. A new algorithm for automatic calculation and optimization was developed.

Let there be a function $f(x, y)$ as in appendix A. The problem is to find at least one "good" point at x with any $y \in Y$. The direct search with just large but finite number of random points in Y may not give a result because of the smallness of the "good" region. On the other hand there is a possibility to exclude most of Y where "good" points are most likely absent.

The idea of the algorithm is as follows. As was discussed in sec. 3.4 the limitation is connected with the uncertainty in the dark matter density which is called $\Delta\Omega$ in this appendix. The limitation is weaker (the "good" region broader) if $\Delta\Omega$ is larger. So if one lets $\Delta\Omega$ be sufficiently large ($\Delta\Omega > \Delta\Omega_0$) it will be easy to find many "good" points (the density d (see appendix A) will be large). With this amount of points one can calculate the regions in Y where they are concentrated. After that one can make Y smaller $Y \to Y'$ so as to leave only regions with large density. After that the average density increases. It allows to find "good" points faster. So one can make $\Delta\Omega$ smaller. This operation can be repeated until $\Delta\Omega$ becames smaller than $\Delta\Omega_0$ which is the required value. The algorithm is illustrated in fig. B.1.

But these iterations may go on indefinitely without arriving to the value $\Delta\Omega_0$ (the loop in the right top part of the figure). It is possible in two cases:

1. The "good" regions with $\Delta\Omega_0$ are absent.

2. The mechanism of the decreasing of Y is not perfect.

So this algorithm is only able to find "good" points in "difficult" regions of x without the guarantee. But this is always the case for numerical methods.

Now let us concentrate on the methods of decreasing Y. In our case it will be just n-dimensional cube with coordinates y_i^n of a point number N. If one has N "good" points

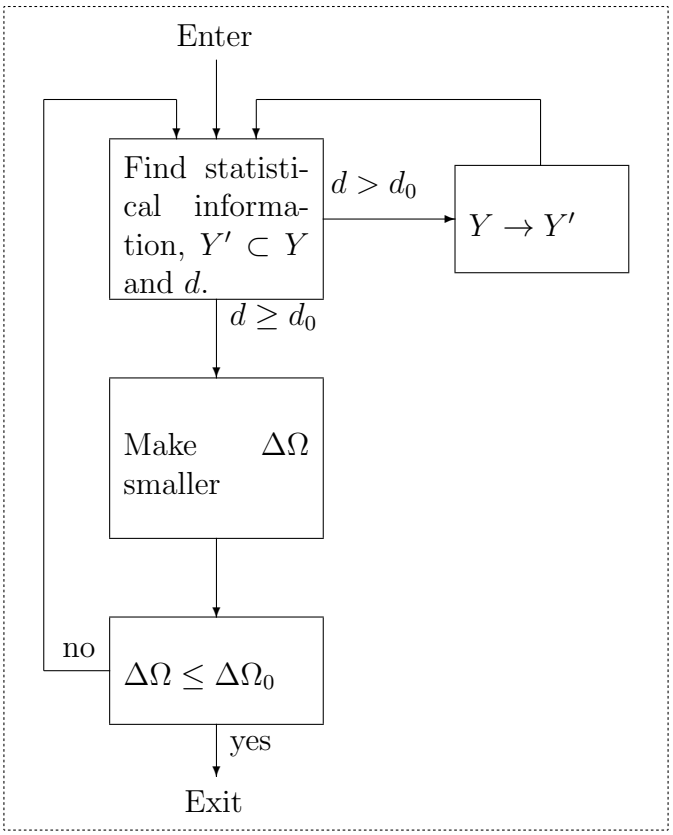

Figure B.1: Algorithm for quick "good" points search.

one can calculate an average value of y_i

$$\langle y_i \rangle = \frac{\sum_{n=1..N} y_i^n}{N} \ , \tag{B.1}$$

and dispersions

$$\langle \Delta y_i^2 \rangle = \frac{\sum_{n=1..N} \Delta y_i^{n2}}{N^2} \ , \tag{B.2}$$

where

$$\Delta y_i^n = y_i^n - \langle y_i^n \rangle \ . \tag{B.3}$$

Then the new Y' may be just a cube with $\langle y_i \rangle \pm \sqrt{\langle \Delta y_i^2 \rangle}$. So if the distribution of "good" points in y_i is flat then $Y = Y'$.

There may be modifications of this method. The problem is that the most part of "good" points with increased $\Delta\Omega$ may be concentrated in an area which is far from the required region $\Omega_0 \pm \Delta\Omega_0$. So the searching for the "comfortable" Y' may be too long. The idea to accelerate it is to take into account a correlation between y_i and Ω. This method was developed and tested but it didn't give an essential advantage for the present calculations. It will not be discussed here.

B.1 Example

The algorithm was realized in fortran77 and tested for allowed points searching from chapter 3. The role of $\Delta\Omega$ is played by $\sigma\Omega_{\rm dark}$. The starting (input) value was $\sigma\Omega_{\rm dark} = 1$. 60 points for statistical information calculations were assumed to be sufficient. y_i were random parameters. The starting Y was the region described in sec. 3.1.

$M^{\pm} = 350 \pm 150$ GeV,
$\log_{10} \tan\beta = 0.5 \pm 1.5$,
$\mu = 450 \pm 250$ GeV,
$\alpha_1 = 0 \pm \pi/2$,
$\alpha_2 = \pi/2 \pm \pi/2$,
$\alpha_3 = \pi/2 \pm \pi/2$.

The "$\pm$" notation for the intervals is used because it will be important to compare the size of final intervals with the starting one. It will also be convenient to move the region of α_1 by $\pi/2$ because in this way the most part of "good" points is concentrated near the center of the region ($\alpha_1 = 0$) but not near the boundaries of it.

Values of the fixed parameters were

$M_1 = 300$ GeV,
$M_2 = 400$ GeV,
$M_\phi = 50$ GeV,
$\eta = 0.6,\ 0.3,\ 0.295, 0.29,\ 0.25, 0.2$.

These values correspond to the boundary of the allowed region in fig. 3.1.

The result is as follows

- $\eta = 0.6$. The allowed point was found after 4 iterations. The Y was not made much smaller than the starting one.
- $\eta = 0.3$. 12 iterations were necessary. The regions for all the random parameters were made smaller by about one order of magnitude.
- $\eta = 0.295$. 28 iterations were necessary. The regions for all the random parameters were made smaller by about one order of magnitude but the last region was especially small, $\log_{10} \tan\beta = 0.807 \pm 0.084$.
- $\eta = 0.29$. After the 13th iteration the $\sigma\Omega_{\rm dark}$ stabilized near $\sigma\Omega_{\rm dark} = 0.0095$ after more than 200 iteration. Allowed point was not found.
- $\eta = 0.25$. A similar result as in the previous case but $\sigma\Omega_{\rm dark}$ was not made smaller than $\sigma\Omega_{\rm dark} = 0.047$.
- $\eta = 0.2$. A similar result, $\sigma\Omega_{\rm dark} = 0.12$.

Another series of results is for the not clear-cut histograms from sec. 3.7. There are many "squares" that are white but not grey just because of a small probability to find a "good" point with the given values of fixed parameters (low density) (see sec. 3.3). For example it is obvious for the "square" $M_1 = 100$ GeV, $M_2 = 400$ GeV, $M_\phi = 80$ GeV and $\eta = 0.3$, see fig. 3.9 where this "square" is surrounded by grey "squares". Indeed a "good" point was easily (very quickly) found during only 5 iterations. By the same way many other "gaps" were filled. But the problem is the program is not able to determine the cases with truly absence of "good" points (zero density). It just works indefinitely. Any criterion of such "unusefulness" of the further iterations may be investigated in the future.

Using this method the allowed points in a region with small density can be found much faster than using the direct search. However if the allowed points are absent it may require much machine time to estimate this fact. In the present case with only 6 random parameters the efficiency of the method is not so evident as it may be in a case with a larger number of arbitrary parameters.

Bibliography

[1] E. W. Kolb and M. S. Turner, *Redwood City, USA: Addison-Wesley (1988) 719 P. (Frontiers in Physics, 70)*

[2] G. Jungman, M. Kamionkowski and K. Griest, Phys. Rept. **267** (1996) 195 [arXiv:hep-ph/9506380].

[3] M. Taoso, G. Bertone and A. Masiero, JCAP **0803** (2008) 022 [arXiv:0711.4996 [astro-ph]].

[4] V. A. Ryabov, V. A. Tsarev and A. M. Tskhovrebov, Phys. Usp. **51** (2008) 1091.

[5] K. G. Begeman, A. H. Broeils and R. H. Sanders, Mon. Not. Roy. Astron. Soc. **249** (1991) 523.

[6] J. Binney and S. Tremaine, arXiv:astro-ph/9304010.

[7] D. Zaritsky, Publ. Astron. Soc. Pac. 394 (1992) 1.

[8] E. Komatsu *et al.* [WMAP Collaboration], Astrophys. J. Suppl. **180** (2009) 330 [arXiv:0803.0547 [astro-ph]].

[9] F. Zwicky, Astrophys. J. **86** (1937) 217.

[10] S. M. Faber and R. E. Jackson, Astrophys. J. **204** (1976) 668.

[11] R. Minchin *et al.*, Astrophys. J. **622** (2005) L21 [arXiv:astro-ph/0502312].

[12] Ciardullo, R., Jacoby, G. H. and Dejonghe, H. B. (sep 1993). "The radial velocities of planetary nebulae in NGC 3379". The Astrophysical Journal 414: 454462. doi:10.1086/173092. http://adsabs.harvard.edu/abs/1993ApJ...414..454C.

[13] A. Vikhlinin, A. Kravtsov, W. Forman, C. Jones, M. Markevitch, S. S. Murray and L. Van Speybroeck, Astrophys. J. **640** (2006) 691 [arXiv:astro-ph/0507092].

[14] D. Clowe, M. Bradac, A. H. Gonzalez, M. Markevitch, S. W. Randall, C. Jones and D. Zaritsky, Astrophys. J. **648** (2006) L109 [arXiv:astro-ph/0608407].

[15] http://www.youtube.com/watch?v=2DoPAeU3a6Yx

[16] http://www.youtube.com/watch?v=Hg2SHngX_D8

[17] J. D. Bekenstein, Nucl. Phys. A **827** (2009) 555C [arXiv:0901.1524 [astro-ph]].

[18] G. Belanger, F. Boudjema, A. Pukhov and A. Semenov, Comput. Phys. Commun. **180** (2009) 747 [arXiv:0803.2360 [hep-ph]].

[19] A. Aguirre, C. P. Burgess, A. Friedland and D. Nolte, Class. Quant. Grav. **18** (2001) R223 [arXiv:hep-ph/0105083].

[20] G. Hinshaw *et al.* [WMAP Collaboration], Astrophys. J. Suppl. **170** (2007) 288 [arXiv:astro-ph/0603451].

[21] D. Scott and G. F. Smoot, arXiv:astro-ph/0601307.

[22] S. Dodelson, "Modern Cosmology," *Amsterdam, Netherlands: Academic Pr. (2003) 440 p*

[23] B. Fields and S. Sarkar, arXiv:astro-ph/0601514.

[24] P. Scott, J. Edsjo and M. Fairbairn, arXiv:0711.0991 [astro-ph].

[25] A. D. Dolgov, Phys. Rept. **370** (2002) 333 [arXiv:hep-ph/0202122].

[26] S. Dodelson and L. M. Widrow, Phys. Rev. Lett. **72** (1994) 17 [arXiv:hep-ph/9303287].

[27] C. T. Hill and E. A. Paschos, Phys. Lett. B **241** (1990) 96.

[28] A. De Rujula, S. L. Glashow and U. Sarid, Nucl. Phys. B **333** (1990) 173.

[29] B. Holdom, Phys. Lett. B **166** (1986) 196.

[30] Z. Chacko, B. Dutta, R. N. Mohapatra and S. Nandi, Phys. Rev. D **56** (1997) 5466 [arXiv:hep-ph/9704307].

[31] K. J. Ahn and P. R. Shapiro, Mon. Not. Roy. Astron. Soc. **363** (2005) 1092 [arXiv:astro-ph/0412169].

[32] E. W. Kolb, D. J. H. Chung and A. Riotto, arXiv:hep-ph/9810361.

[33] A. E. Faraggi, K. A. Olive and M. Pospelov, Astropart. Phys. **13** (2000) 31 [arXiv:hep-ph/9906345].

[34] M. Ambrosio *et al.* [MACRO Collaboration], Eur. Phys. J. C **25** (2002) 511 [arXiv:hep-ex/0207020].

[35] L. B. Okun, Phys. Usp. **50** (2007) 380 [arXiv:hep-ph/0606202].

[36] A. Y. Ignatiev and R. R. Volkas, Phys. Lett. B **487** (2000) 294 [arXiv:hep-ph/0005238].

[37] U. Seljak, A. Makarov, P. McDonald and H. Trac, Phys. Rev. Lett. **97** (2006) 191303 [arXiv:astro-ph/0602430].

[38] K. Griest, Astrophys. J. **366** (1991) 412.

[39] D. J. Hegyi and K. A. Olive, Phys. Lett. B **126** (1983) 28.

[40] C. Alcock *et al.* [MACHO Collaboration], Phys. Rev. Lett. **74** (1995) 2867 [arXiv:astro-ph/9501091].

[41] M. S. Turner, Phys. Rept. **197** (1990) 67.

[42] G. G. Raffelt, Phys. Rept. **198** (1990) 1.

[43] S. Desai *et al.* [Super-Kamiokande Collaboration], Phys. Rev. D **70** (2004) 083523 [Erratum-ibid. D **70** (2004) 109901] [arXiv:hep-ex/0404025].

[44] M. Ambrosio *et al.* [MACRO Collaboration], Phys. Rev. D **60** (1999) 082002 [arXiv:hep-ex/9812020].

[45] M. M. Boliev, A. V. Butkevich, A. E. Chudakov, S. P. Mikheev, O. V. Suvorova and V. N. Zakidyshev, *Contributed to the 24th International Cosmic Rays Conference (ICRC 95), 28 Aug - 8 Sep 1995, Rome, Italy*

[46] V. Aynutdinov *et al.*, Nucl. Instrum. Meth. A **588** (2008) 99.

[47] S. W. Barwick *et al.* [HEAT Collaboration], Astrophys. J. **482** (1997) L191 [arXiv:astro-ph/9703192].

[48] L. Bergstrom, J. Edsjo and P. Ullio, Astrophys. J. **526** (1999) 215 [arXiv:astro-ph/9902012].

[49] A. W. Strong, H. Bloemen, R. Diehl, W. Hermsen and V. Schoenfelder, Astrophys. Lett. Commun. **39** (1999) 209 [arXiv:astro-ph/9811211].

[50] G. Bertone, Astrophys. Space Sci. **309** (2007) 505 [arXiv:astro-ph/0608706].

[51] G. Weidenspointner *et al.*, arXiv:astro-ph/0702621.

[52] M. Pospelov and A. Ritz, Phys. Lett. B **651** (2007) 208 [arXiv:hep-ph/0703128].

[53] A. Kusenko and M. E. Shaposhnikov, Phys. Lett. B **418** (1998) 46 [arXiv:hep-ph/9709492].

[54] C. D. Froggatt and H. B. Nielsen, Phys. Lett. B **368** (1996) 96 [arXiv:hep-ph/9511371].

[55] A. M. Polyakov, JETP Lett. **20** (1974) 194 [Pisma Zh. Eksp. Teor. Fiz. **20** (1974) 430].

[56] E. Witten, Phys. Rev. D **30** (1984) 272.

[57] T. Saito, Y. Hatano, Y. Fukada and H. Oda, Phys. Rev. Lett. **65** (1990) 2094.

[58] E. Farhi and R. L. Jaffe, Phys. Rev. D **30** (1984) 2379.

[59] F. D. Steffen, *In the Proceedings of 2005 International Linear Collider Workshop (LCWS 2005), Stanford, California, 18-22 Mar 2005, pp 0705* [arXiv:hep-ph/0507003].

[60] J. L. Feng, A. Rajaraman and F. Takayama, Phys. Rev. Lett. **91** (2003) 011302 [arXiv:hep-ph/0302215].

[61] J. G. Skibo *et al.*, arXiv:astro-ph/9704207.

[62] L. Hui, Phys. Rev. Lett. **86** (2001) 3467 [arXiv:astro-ph/0102349].

[63] B. Grzadkowski and P. Osland, arXiv:0910.4068 [hep-ph].

[64] B. Grzadkowski, O. M. Ogreid and P. Osland, Phys. Rev. D **80** (2009) 055013 [arXiv:0904.2173 [hep-ph]].

[65] P. Osland, P. N. Pandita and L. Selbuz, Phys. Rev. D **78** (2008) 015003 [arXiv:0802.0060 [hep-ph]].

[66] W. Grimus, L. Lavoura, O. M. Ogreid and P. Osland, Nucl. Phys. B **801** (2008) 81 [arXiv:0802.4353 [hep-ph]].

[67] W. Grimus, L. Lavoura, O. M. Ogreid and P. Osland, J. Phys. G **35** (2008) 075001 [arXiv:0711.4022 [hep-ph]].

[68] A. W. El Kaffas, O. M. Ogreid and P. Osland, *In the Proceedings of 2007 International Linear Collider Workshop (LCWS07 and ILC07), Hamburg, Germany, 30 May - 3 Jun 2007, pp HIG08* [arXiv:0709.4203 [hep-ph]].

[69] A. Wahab El Kaffas, P. Osland and O. M. Ogreid, Phys. Rev. D **76** (2007) 095001 [arXiv:0706.2997 [hep-ph]].

[70] A. W. El Kaffas, P. Osland and O. M. Ogreid, Nonlin. Phenom. Complex Syst. **10** (2007) 347 [arXiv:hep-ph/0702097].

[71] A. W. El Kaffas, W. Khater, O. M. Ogreid and P. Osland, Nucl. Phys. B **775** (2007) 45 [arXiv:hep-ph/0605142].

[72] W. Khater and P. Osland, Nucl. Phys. B **661** (2003) 209 [arXiv:hep-ph/0302004].

[73] N. G. Deshpande and E. Ma, Phys. Rev. D **18** (1978) 2574.

[74] I. F. Ginzburg and I. P. Ivanov, arXiv:hep-ph/0312374.

[75] P. Gambino and M. Misiak, Nucl. Phys. B **611** (2001) 338 [arXiv:hep-ph/0104034].

[76] K. Cheung and O. C. W. Kong, Phys. Rev. D **68** (2003) 053003 [arXiv:hep-ph/0302111].

[77] V. D. Barger, J. L. Hewett and R. J. N. Phillips, Phys. Rev. D **41** (1990) 3421.

[78] [ALEPH Collaboration and DELPHI Collaboration and L3 Collaboration and], Phys. Rept. **427** (2006) 257 [arXiv:hep-ex/0509008].

[79] G. W. Bennett *et al.* [Muon g-2 Collaboration], Phys. Rev. Lett. **92** (2004) 161802 [arXiv:hep-ex/0401008].

[80] C. Newton and T. T. Wu, Z. Phys. C **62** (1994) 253.

[81] E. Ma, Int. J. Mod. Phys. A **16** (2001) 3099 [arXiv:hep-ph/0101355].

[82] G. Belanger, F. Boudjema, A. Pukhov and A. Semenov, arXiv:1005.4133 [hep-ph].